# Geospatial Time Series Analysis for Coastal Systems: AI-Powered NARX Neural Networks Integrating Remote Sensing for Advanced Shoreline Change Prediction

Nada Mansour<sup>1,2,\*</sup>, Tharwat Sarhan<sup>1</sup>, Mahmoud El-Gamal<sup>1</sup>, Karim Nassar<sup>1</sup>, Mahmoud Abd-Elmaboud<sup>1,\*</sup>

# **Highlights**

- Advanced NARX neural network with Bayesian optimization achieved exceptional shoreline prediction accuracy (RMSE: 0.07-0.52m).
- ➤ Integration of multi-temporal Landsat data (1987-2022) enabled precise shoreline delineation across 158 transects with NRMSE of 0.116595.
- Model 5's multi-parameter integration (wave height, tidal range, displacement) demonstrated superior performance with Performance Index values ranging from 0.000149 to 0.000857.
- > Spatial analysis quantified critical erosion zones (-7.0 m/year) and accretion areas (+24.48 m/year) across 21 distinct coastal sectors.
- The decision matrix enabled targeted protection strategies based on vulnerability thresholds ( $\pm 20$  m/year High,  $\pm 5$ -20 m/year Moderate,  $\pm 0$ -5 m/year Low).
- The implementation framework aligns with SDGs through data-driven coastal protection and climate adaptation strategies.

<sup>&</sup>lt;sup>1</sup> Irrigation and Hydraulic Engineering Dept., Faculty of Engineering, Mansoura University, Egypt.

<sup>&</sup>lt;sup>2</sup> Assistant lecturer, Mansoura Higher Institute of Engineering and Technology, Egypt.

<sup>\*</sup>Corresponding author at Irrigation and Hydraulics Department, Faculty of Engineering, Mansoura University, Egypt

#### **Abstract**

Accurate shoreline prediction models are crucial for coastal management under increasing climate change pressures. This study presents an advanced approach combining Nonlinear Autoregressive with Exogenous inputs (NARX) neural networks optimized through modified Levenberg-Marquardt algorithms with Bayesian regularization, integrating multi-temporal remote sensing data to predict shoreline evolution. Focusing on a 35-km stretch of Egypt's Nile Delta coastline, five NARX models are developed and compared, incorporating different combinations of significant wave height (<4m), tidal range (-0.10 to 0.85m), and historical shoreline displacement data. The methodology integrated 35 years (1987-2021) of Landsat imagery with hydrodynamic parameters across 158 transects at 215-m intervals. Results demonstrated that the integrated model combining all three parameters achieved exceptional accuracy, with Root Mean Square Error (RMSE) values of 0.07m (2012) to 0.52m (2021) and Nash-Sutcliffe efficiency ranging from 0.95664 to 0.999377, significantly outperforming single-parameter models. Cross-correlation analysis revealed stronger relationships between shoreline changes and combined parameters. The novel Performance Index (0.000149 to 0.000857) validated the integrated approach's superiority. The spatial analysis identified 21 distinct sectors with critical erosion zones (-7.0 m/year) and accretion areas (+24.48 m/year), enabling targeted protection strategies based on quantified vulnerability thresholds. This research advances shoreline prediction methodology through enhanced parameter integration, providing a robust framework for coastal management under climate change conditions. The findings support sustainable coastal development and climate adaptation strategies in vulnerable delta regions.

**Keywords:** Shoreline Prediction; NARX Neural Network; Remote Sensing; Coastal Morphodynamics; Nile Delta.

# 1 Shoreline extraction (1987-2022) Tidal range Significant wave height (Contains Alamquin Controlls) Alamquin Controlls Ala

# **Graphical abstract**

#### 1. Introduction

Coastal shorelines, the dynamic interfaces between terrestrial and aquatic ecosystems, are subject to complex geomorphological processes operating across various temporal and spatial scales (Vitousek et al. 2017; Masria et al. 2022). Their evolution is governed by both anthropogenic and natural forces, with long-term changes primarily attributed to shifts in relative elevation and sea-level rise (Vousdoukas et al. 2020; El-Asmar et al. 2024). Short-term sediment redistribution is predominantly driven by the combined effects of wave action, nearshore currents, and fluvial processes (Youssef et al. 2024). This constant flux results in continuous coastline reshaping through erosion and accretion, necessitating precise shoreline position estimates for effective erosion mitigation strategies (Calkoen et al. 2021; Abd-Elaty et al. 2024). Accurate forecasting of shoreline configurations requires a comprehensive understanding of historical and current coastal dynamics (Zeinali et al. 2021; Mansour et al. 2024). This study examines shoreline movements along the North Delta coast, specifically the stretch between the Kitchener drain and the Gamsa outlet, characterized by highly dynamic deltaic beaches (ElKotby et al. 2024). These geomorphic systems undergo continuous transformations across multiple geographical and temporal scales (Luijendijk et al. 2018; Ibrahim et al. 2024).

The field of coastal geomorphology has witnessed significant advancements in shoreline change analysis techniques over the past two decades. The Digital Shoreline Analysis System (DSAS), leveraging multi-temporal satellite data, has emerged as a cornerstone for analyzing shoreline dynamics (Nandi et al. 2016; Hagenaars et al. 2018; Bhuyan et al. 2023). Integrating remote sensing and Geographical Information Systems (GIS) technologies has revolutionized shoreline change assessments, enabling unprecedented spatial and temporal coverage (Luijendijk et al. 2018; Raja et al. 2023). Recent studies have demonstrated the potential of combining traditional DSAS approaches with Machine Learning (ML) techniques to improve prediction accuracy (Calkoen et al. 2021; Zeinali et al. 2021). However, most existing models have focused on single-parameter approaches, highlighting the need for integrated multi-parameter prediction systems (Vitousek et al. 2023).

Integrating numerical models with remote sensing data has significantly advanced shoreline prediction capabilities (Vitousek et al. 2023). Traditional approaches like the End Point Rate (EPR) and Linear Regression (LRR) models have been widely used for shoreline predictions (Calkoen et al. 2021). However, these methods often fail to capture complex temporal patterns and nonlinear relationships in coastal systems (Zeinali et al. 2021). Recent ML approaches have demonstrated superior performance in handling such complexities (Goldstein et al. 2020; Montaño et al. 2020). The efficacy of these predictive models depends on multiple factors, including data quality, temporal resolution, and the incorporation of relevant physical parameters (Luijendijk et al. 2018).

Shoreline change analysis has evolved significantly from traditional Geographic Information System (GIS) approaches to sophisticated ML techniques (Calkoen et al. 2021). While conventional tools like DSAS remain valuable for basic analysis, they show limitations in processing large datasets and capturing complex temporal patterns

(Vitousek et al. 2023). Recent advances in deep learning have enabled more accurate shoreline detection and prediction capabilities (Goldstein et al. 2020). Neural network approaches, particularly recurrent architectures, have demonstrated superior performance in capturing temporal dependencies in coastal systems (Vidyalashmi et al. 2024a). These methods can process multiple input parameters simultaneously, offering advantages over traditional single-parameter approaches (Montaño et al. 2020). Integrating ML with remote sensing data has enabled global near-real-time monitoring of coastal changes (Luijendijk et al. 2018; Vos et al. 2019). This advancement is particularly relevant for sustainable coastal management and climate change adaptation strategies (Vousdoukas et al. 2020). Neural network approaches have shown particular promise in combining multiple environmental parameters, including wave characteristics, tidal patterns, and historical shoreline positions (Huang et al. 2024a).

The NARX (Nonlinear Auto-Regressive with Exogenous Input) architecture has emerged as a powerful tool for environmental time series prediction by addressing key limitations of traditional forecast methods (Tang 2020). Unlike conventional approaches that process temporal data sequentially, NARX networks employ multilevel feedback connections that enable the simultaneous integration of historical states and external forcing factors (Hewamalage et al. 2021). This architectural advantage is particularly relevant for coastal systems, where shoreline evolution results from complex interactions between multiple time-varying parameters. The network's ability to capture both short-term fluctuations and long-term trends while maintaining computational efficiency makes it especially suitable for coastal prediction tasks (Vos et al. 2019). Recent applications have demonstrated NARX's superior performance in handling nonlinear relationships and temporal dependencies in environmental data (Vidyalashmi et al. 2024b), suggesting its potential for improving shoreline prediction accuracy through multi-parameter integration.

Despite advances in ML applications for coastal systems, significant challenges remain in developing computationally efficient models that integrate multiple environmental parameters while maintaining high accuracy in prediction (Huang et al. 2024b). While recent studies have explored various ML techniques in coastal engineering (Vitousek et al. 2023), most focus on single-parameter predictions or limited temporal scales (Simmons et al. 2017). Integrating multiple time-varying parameters with historical shoreline data remains particularly challenging (Splinter and Coco 2021).

This research advances shoreline prediction methodology by developing an integrated NARX-based framework that addresses key limitations in existing approaches. While previous studies have largely relied on single-parameter predictions or limited temporal scales, this study introduces a comprehensive multi-parameter approach incorporating historical displacement data, significant wave height, and tidal range. The investigation focuses on a 40-km stretch of Egypt's Nile Delta coastline between the Kitchener drain and Gamsa outlet. This region exemplifies the complex interactions between natural coastal processes and anthropogenic pressures. The research makes three primary contributions: (1) the development of a novel integrated prediction framework that demonstrates superior accuracy over traditional single-parameter approaches, (2) the quantification of the relative importance of different environmental parameters in

shoreline prediction, and (3) the establishment of a methodological foundation for incorporating multiple time-varying parameters in coastal evolution models. These advances provide both theoretical insights into coastal morphodynamics and practical tools for sustainable coastal management under changing climate conditions.

# 2. Material and methods

# 2.1. Study Area

The study area, situated along the Mediterranean coast of Egypt's Nile Delta (Figure. 1a), spans approximately ~35 km westward from the Kitchener drain to the Gamsa Inlet, encompassing coordinates 31°11'9.47"E to 31°33'48.35"E and 31°34'56.56"N to 31°33'48.35"N. This region exhibits extensive land prone to erosion, accretion, and vulnerable coastal activities. As shown in Figure. 1b, the study area is divided into distinct zones featuring critical infrastructure, including New Mansoura City, a desalination plant, and popular coastal destinations such as Baltim and Gamsa Beach.

The hydrodynamic characteristics of the study area have been continuously monitored using the S4DW method (Trageser and Elwany 1990), recording the directed wave spectrum hourly at a water depth of 12 m. Dominant seasonal waves originate from the north to northwest and are characterized by consistent heights around 120 cm and 6-9 seconds durations. Winter storms, occurring at least annually between November and April, exhibit higher wave heights up to 2.70 m with periods of 7-9 seconds and maximum wave heights reaching 4.00 m. Longshore currents, measured between the breaker line and coast at water depths of 1.30-2.0 m, align with wave motion and reach peak velocities during high storm wave periods (Mansour et al. 2024).

Wind analysis (2011-2012) reveals prevailing NW and WNW directions contributing 50-60% of total wind energy, with average speeds ranging from 2-9 m/s in summer to 9-13 m/s in spring (Frihy and El-Sayed 2013; Mansour et al. 2024). Completing the High Aswan Dam in 1964 marked a critical turning point, substantially reducing sediment discharge at the Nile promontories (Stanley and Warne 1998; El-Sharnouby et al. 2020). This reduction intensified erosive forces along the coastline, necessitating protection measures. In response, the western side of the drain was reinforced with 15 groins to combat continuous erosion rates of approximately 20 meters per year (El-Sharnouby et al. 2020; Dewidar and Bayoumi 2021).

The digitized shorelines for multiple years between 1987 and 2022 (Figure. 1c) reveal significant morphological changes along the coastline. These temporal variations demonstrate the oblique inclination of the shoreline in this area compared to the Kitchener zone to the west, highlighting the region's dynamic nature of coastal processes (Abd-Elhamid et al. 2023). The shoreline evolution patterns visible in the digitized data reflect both natural processes and anthropogenic interventions over the study period (Tharwat Sarhan et al. 2022). Recent interventions include the installation of an additional 17 groins along the drain's eastern shoreline in early 2022, aiming to reduce downstream erosion and enhance long-term coastal stability (Masria et al. 2024). This ongoing coastal protection program demonstrates the continued vulnerability of

this stretch of coastline to erosion processes (ElKotby et al. 2023).

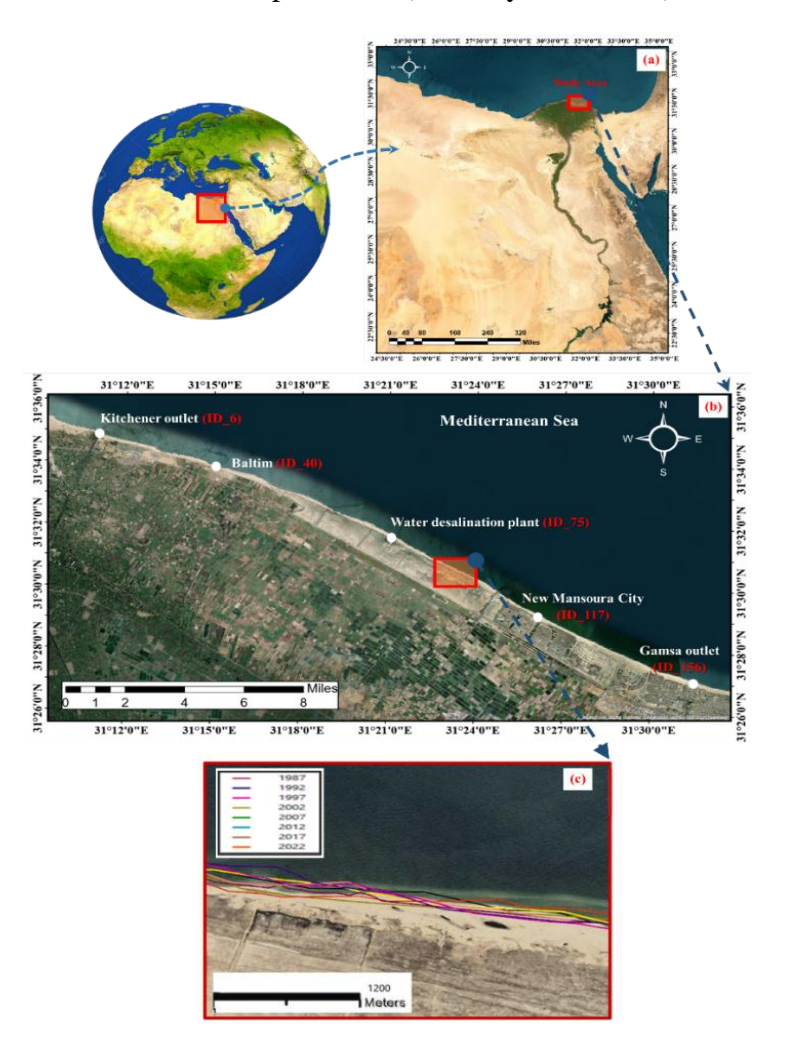


**Figure.1 a** Location of the study area; **b** Shoreline with a length of ~35 km with the location of hazard cities with a number of transect IDs; **c**The digitized for the previous studied years.

### 2.2. Research Methodology

The comprehensive methodological framework of this study, as illustrated in Figure. 2, encompasses several integrated analytical approaches for shoreline prediction and evolution analysis. The methodology builds upon established remote sensing techniques while incorporating hydrodynamic parameters and ML predictions through the following key stages:

1. Data Acquisition and Processing: The initial phase involves analysis of multitemporal Landsat satellite imagery (1987-2022), including systematic preprocessing through radiometric calibration, atmospheric correction, and Tasseled

- Cap Transformation for enhanced shoreline delineation, culminating in the establishment of 158 shore-perpendicular transects at 215 m intervals along the ~35 km study area.
- 2. Neural Network Implementation: This phase focuses on the development of five distinct NARX (Nonlinear Autoregressive with Exogenous inputs) models, integrating significant wave height measurements, tidal range data, and historical shoreline positions, with the dataset strategically partitioned into training (70%, 1987-2010) and testing (30%, 2010-2021) segments.
- 3. Model Development and Validation: The modeling phase involves implementing varying input parameter combinations across models, validated through comprehensive statistical metrics, including RMSE, MAPE, Nash-Sutcliffe Efficiency, and Performance Index.
- 4. Impact Assessment: The final stage encompasses analysis of predicted shoreline positions, evaluation of coastal vulnerability, assessment of climate change implications, and generation of insights for coastal management strategies.

This systematic approach enables quantitative analysis of shoreline dynamics while accounting for complex interactions between coastal processes, climate factors, and anthropogenic influences. The following sections detail each methodological component, their implementation, and their role in understanding coastal evolution patterns.

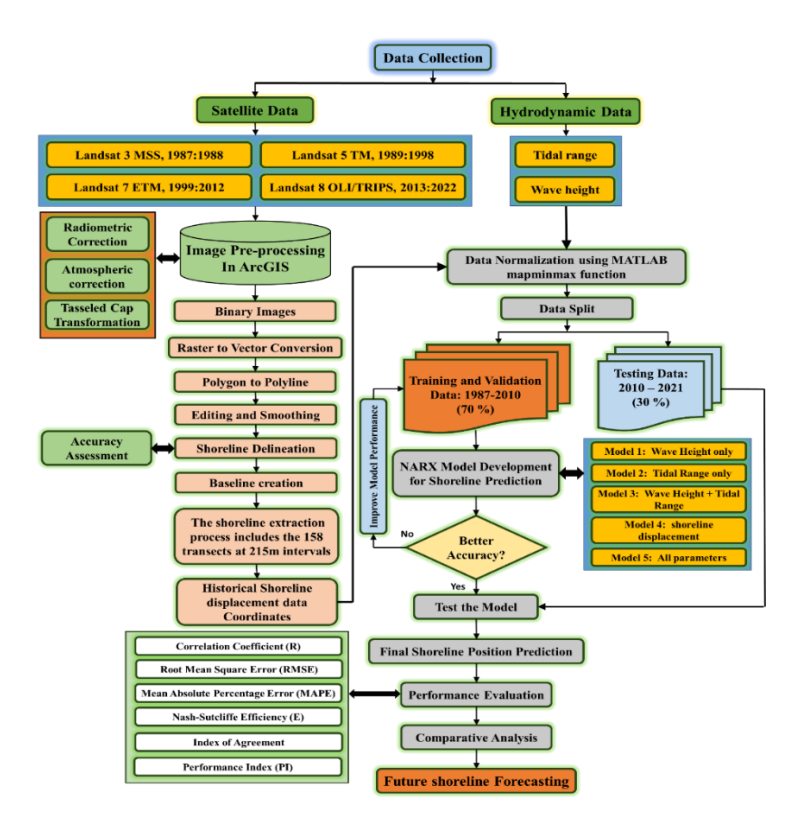


**Figure. 2** Methodological framework for shoreline prediction using a NARX neural network.

#### 2.2.1. Data Source

Accurately monitoring and analyzing shoreline dynamics requires high-quality satellite imagery with consistent spatial and temporal resolution. This study utilized multi-temporal satellite data spanning 35 years (1987-2022) from multiple Landsat missions, including the Landsat-1 Multispectral Scanner (MSS), Landsat-4 and -5 Thematic Mapper (TM), Landsat-7 Enhanced Thematic Mapper (ETM), and Landsat-8 Operational Land Imager and Thermal Infrared Sensor (OLI-TIRS). The imagery was acquired through the United States Geological Survey (USGS) Earth Explorer platform, providing a comprehensive dataset for analyzing long-term coastal changes (Table 1).

The selection of Landsat imagery was particularly appropriate for this study due to its moderate spatial resolution (30m), consistent temporal coverage, and extensive historical archive (Wulder et al. 2019). The study area's moderate tidal range minimizes the influence of tidal variations on shoreline position extraction from satellite data, enhancing the reliability of shoreline delineation (Boak and Turner 2005). Image processing and shoreline extraction were conducted using ArcGIS 10.8, following established protocols for automated shoreline detection in coastal environments (Hagenaars et al. 2018; Vos et al. 2019). All satellite scenes underwent rigorous quality assessment to ensure cloud cover was below 10%, and images were acquired during similar tidal conditions to maintain consistency in shoreline detection. This methodological approach aligns with recent advances in satellite-based coastal monitoring and provides a robust foundation for analyzing multi-decadal shoreline changes in the study area.

**Table 1.** Technical specifications and characteristics of satellite imagery used in the study (1987-2022).

Year	Spacecra ID	Sensor ID	Path /Row	Coordinate System/ Datum	Spatial resolution (m)	Spectral Bands Used	Cloud Cover (%)	Size (Row/ Path)
1987	LAND SAT_1	MSS						
1992	LAND SAT_4							
1994	LAND SAT_5	TM						
1997	LAND SAT_5		178/3 9	UTM/WG S 84	30	3,4, and 5	< 10%	178/39
1999	LAND SAT_7							
2002	LAND SAT_7	ETM						
2007	LAND SAT_7							

2012	LAND SAT_7				
2017	LAND SAT_8	OLI_			
2022	LAND SAT_8	TRIS			

The hydrodynamic characteristics of the study area, crucial for understanding coastal processes, are illustrated in Figure. 3. Throughout the research period, significant wave height (H<sub>s</sub>) predominantly remained below four meters. In comparison, tidal levels fluctuated between -0.10 and 0.85 meters, demonstrating the dynamic nature of the coastal environment (Nielsen and Callaghan 2003). These datasets were meticulously documented monthly, providing a comprehensive temporal resolution for analysis. H<sub>s</sub> measurements were conducted offshore, complemented by hourly hindcast wave data up to 2020, provided by the Beach Research Center. This approach aligns with best practices in coastal hydrodynamics research, ensuring a robust dataset for analysis (Kamphuis 2010). To account for astronomical tides, the T Tide software package was employed to analyze water level data from 1990 to 2020, a method widely recognized in tidal studies for its accuracy and reliability (Pawlowicz et al. 2002). This multifaceted approach to data collection and analysis, incorporating both shoreline changes and hydrodynamic factors, provides a comprehensive foundation for understanding the complex coastal dynamics of the study area. Integrating these diverse datasets enables a more nuanced and accurate assessment of shoreline evolution and its driving forces.

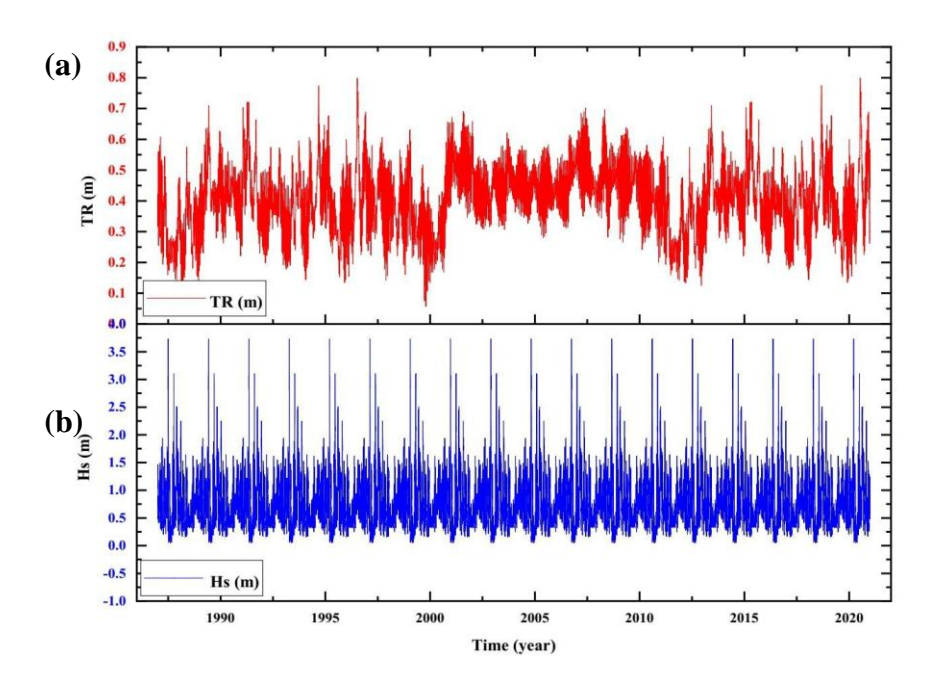


**Figure. 3 a** Tidal range; **b** Significant wave height in the study area over the period.

#### 2.2.2. Shoreline extraction and uncertainty evaluation

The extraction of shorelines from medium-resolution satellite imagery presents significant challenges due to the presence of a water-saturated zone at the land-water interface. This study implemented a systematic approach to shoreline delineation using Landsat imagery, specifically focusing on Band 5 (Short-Wave Infrared) due to its optimal spectral characteristics for water-land boundary discrimination (Figure. 4). The methodology leverages water bodies' distinct spectral reflectance properties, which exhibit minimal reflectance in the SWIR spectrum compared to other land cover types (Boak and Turner 2005; Hagenaars et al. 2018).

The shoreline extraction process was executed through a semi-automated workflow in ArcGIS 10.6.1, comprising three primary stages: (1) conditional value calculation using a raster calculator to identify the dry/wet line based on reflectance thresholds, (2) raster-to-polygon conversion for spatial delineation, and (3) polyline generation for continuous shoreline representation. The resultant shorelines were georeferenced using the WGS\_1984\_UTM\_Zone\_36N coordinate system to ensure spatial accuracy and compatibility with other geospatial datasets.

The 2022 shoreline extractions underwent additional processing and comparative analysis for validation and uncertainty assessment. A baseline was established at 500-meter intervals using a buffering approach, from which shore-perpendicular transects were generated to quantify shoreline positions and temporal changes. The accuracy of the shoreline detection methodology was evaluated using the normalized root mean square error (NRMSE). Three different pixel threshold values were tested: 14,000, 15,000, and 16,000, yielding NRMSE values of 0.227181, 0.290475, and 0.116595, respectively. The optimal threshold of 16,000 produced the lowest NRMSE (0.116595), indicating superior accuracy in shoreline delineation (Vos et al. 2019; Mansour et al. 2024). This dimensionless error metric enables robust comparison of shoreline detection accuracy across different spatial and temporal scales. The extracted shorelines were stored in shapefile format, facilitating subsequent analysis of coastal morphodynamics and enabling integration with other spatial datasets for comprehensive coastal change assessment.



**Figure. 4** The methodology for shoreline extraction in 2022 includes; **a** Landsat raster image of Band 5; **b** the binary image; **c** the vector map (polygon shapefile).

# 2.2.3. Data Preparation and Model Development

The foundation of robust predictive modeling lies in meticulous data preparation and appropriate model architecture design. Building on established practices in ML applications, five distinct models were developed with different combinations of input parameters, as detailed in Table 2. M (1) utilizes only significant wave height (Hs), M (2) incorporates tidal range (TR), while M (3) combines both parameters. M (4) relies solely on historical shoreline displacement data (ds), and M (5) integrates all three parameters (ds, Hs, TR) with a lag-2 value to capture temporal dependencies. The dataset was strategically partitioned into two segments: a training set spanning 1987-2010 (70% of data) and a test set covering 2010-2021 (30% of data), following standard procedures for neural network applications (Beale et al. 2010). Data normalization was implemented using MATLAB's mapminmax function to ensure optimal model performance.

For comprehensive spatial analysis, 158 transects were established at 215-meter intervals along a ~35 km baseline, with special attention given to five high-risk locations (IDs 6, 40, 75, 117, and 156), as shown in Figure. 1b, corresponding to residential areas particularly vulnerable to erosion. Figure. 5 illustrates the temporal evolution of shoreline positions at these critical locations, demonstrating significant variability in shoreline displacement patterns over 34 years. The time series data shows distinct characteristics at each location, with some areas exhibiting greater fluctuations than others, highlighting the complex nature of shoreline dynamics that the models need to capture. This systematic approach to data preparation and organization provides a robust foundation for implementing NARX neural network models, ensuring that both spatial and temporal variations in shoreline behavior are adequately represented in the training and testing datasets.

Models **Mathematical expression** Output Input M(1) $H_s$  $d_s(t) = f(H_s(t-1); H_s(t-2))$  $d_s(t)$ M(2) $d_s(t) = f(T_R(t-1); T_R(t-2))$  $T_R$  $d_s(t)$ M(3) $d_s(t) = f(H_s(t-1); H_s(t-2); T_R(t-1); T_R(t-2))$  $H_s$ ,  $T_R$  $d_s(t)$ M(4) $d_s(t) = f(d_s(t-1); d_s(t-2))$ ds  $d_s(t)$ M(5) $d_s(t) = f(d_s(t-1); d_s(t-2); H_s(t-1); H_s(t-2); T_R(t-1); ds, H_s, T_R$  $d_s(t)$  $T_R(t-2)$ 

Table 2 Summary of model trained and tested.

**Note:**  $d_s$  is the shoreline displacement,  $H_s$  is the significant wave height, and  $T_R$  is the tidal range.

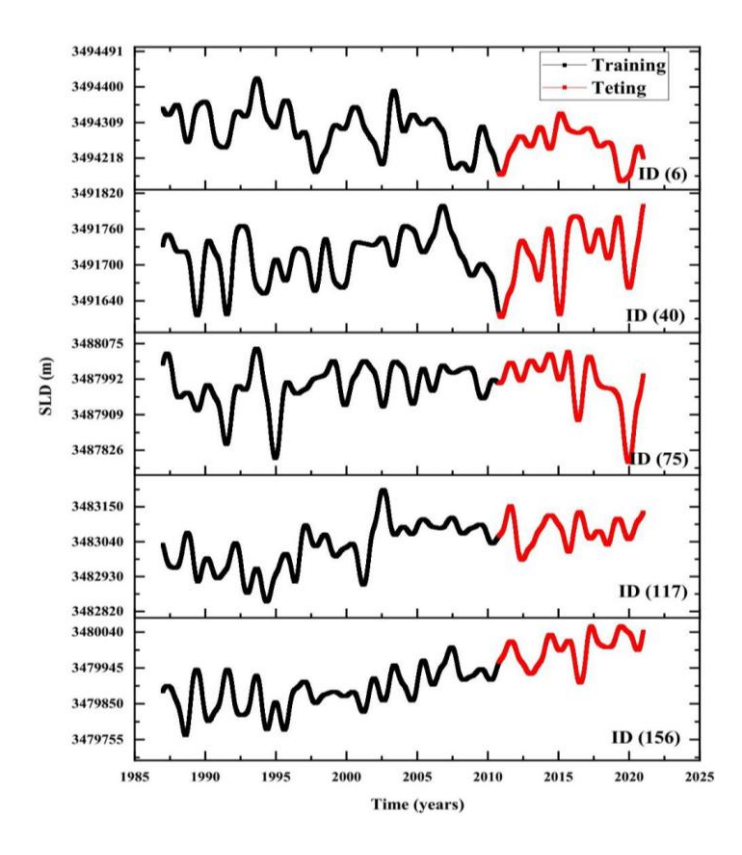


**Figure. 5** Validation and Test for shoreline displacement with time (1987 to 2022) at selected ID of hazard areas.

#### 2.2.4. Nonlinear Autoregressive with Exogenous Input (NARX) Model

A sophisticated nonlinear ML-based model has been implemented to predict shoreline displacement, leveraging both single and multivariate time-series data through advanced neural network techniques (Karunarathna et al. 2016). This approach, known as the Nonlinear Autoregressive with exogenous inputs (NARX) model, has demonstrated significant efficacy in capturing complex coastal dynamics (Hashemi et al. 2010). The neural network architecture comprises an input layer, one or more hidden layers, and an output layer (Figure. 6), a structure well-suited for modeling nonlinear systems like coastal processes (Pardo-Igúzquiza et al. 2019). The model's predictive capability is enhanced by its utilization of historical values, with the number of steps taken at the previous time considered contingent upon the input characteristics and feedback delay (Sahoo and Bhaskaran 2019). Weights assigned to inputs quantify their influence on the output, allowing the model to capture the nuanced interplay of factors affecting shoreline displacement.

Central to the NARX model's effectiveness is selecting an optimal lag value, determined through auto-correlation and correlation functions. These statistical tools measure the similarity between data points across different time intervals, ensuring the model captures relevant temporal relationships in shoreline evolution (Torres-Freyermuth et al. 2017). The term "auto-regression" in the model's name reflects its

ability to account for the influence of past shoreline positions on current and future states.

The general equation of the NARX model, as described by (Torres-Freyermuth et al. 2017), is represented as:

$$\hat{y}(t) = f\left(y(t-1), y(t-2), \dots, y(t-n_y), u(t), u(t-1), u(t-1), u(t-2), \dots, u(t-n_u)\right) + e(t)$$
(1)

where f(.) denotes the neural network mapping function,  $\hat{y}(t)$  is the target variable (predicted shoreline position),  $y(t-n_y)$  is the predictor variable (historical shoreline data), u(t) represents exogenous inputs (e.g., wave height, tidal range),  $n_y$  and  $n_u$  are the respective time delays and e(t) is the model error between target and prediction.

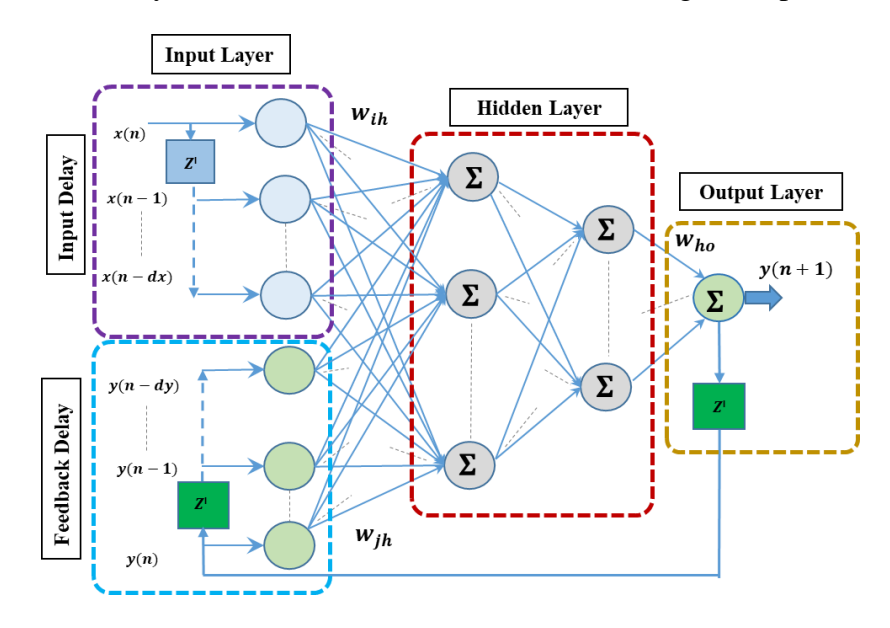


**Figure. 6** Architecture of the NARX neural network showing input layer with input and feedback delays, hidden layer with processing nodes, and output layer.

According to the input variable u(t), the hidden layer output  $H_i$  at time t is obtained as (Chan et al., 2015):

$$H_i(t) = f_1 \left[ \sum_{r=0}^{n_u} w_{ir} u(t-r) + \sum_{l=1}^{n_y} w_{il} y(t-l) + a_i \right]$$
 (2)

where  $w_{ir}$  is the connection weight between input neuron u(t-r) and ith hidden neuron,  $w_{il}$  is the connection weight between the ith hidden neuron and output feedback neuron y(t-l),  $a_i$  is the bias of the ith hidden neuron, and  $f_l(\cdot)$  is the hidden layer activation function. The final prediction can be given by combining the hidden layer outputs:

$$\hat{y}_j(t) = f_2 \left[ \sum_{i=1}^{n_h} w_{ji} H_i(t) + b_j \right]$$
(3)

where wji is the connection weight between the *ith* hidden neuron and *jth* predicted output,  $b_j$  is the bias of the *jth* predicted output,  $n_h$  is the number of hidden neurons, and  $f_2(\cdot)$  is the output layer activation function.

The model's predictive capability is enhanced by its utilization of historical values, with the number of previous time steps considered being contingent upon the input characteristics and feedback delay (Sahoo and Bhaskaran, 2019). Weights assigned to inputs quantify their influence on the output, allowing the model to capture the nuanced interplay of factors affecting shoreline displacement.

# 2.2.5. Modified Levenberg-Marquardt (LM) Training Algorithm

To optimize the NARX network parameters, the Levenberg-Marquardt (LM) algorithm is implemented as the training mechanism due to its superior convergence speed and reliability. The LM algorithm combines the Gauss-Newton algorithm's (GNM) acceleration with the stability of the steepest descent method (SDM), making it particularly effective for training neural networks (Revanesh et al. 2024). LM shifts between the SDM and GNM, as follows (Abd-Elmaboud et al. 2021):

$$\delta = [J^T . J + \lambda . I]^{-1} . J^T . E \tag{4}$$

where J is the Jacobian matrix for the first error term derivatives, T is the Jacobian matrix's transpose,  $\delta$  is the various weighted adjustments, l is a factor, I is the identity matrix, and E is a vector of the output errors.

The LM method sticks to the nearest local minima in complex high-dimensional solution spaces. Training the NARX to the deepest local minimum, i.e., catching near zeros for all Jacobean matrix components, virtually leads to overfitting. The problem is solved by combining Bayesian regularization with LM. In the objective function, add a penalty proportionate to NARX weights. This reduces weights, so the expected output is smoother. A description of the modified objective function, F, is as follows (Kayri 2016; Shang et al. 2023):

$$F = \beta F_D + \alpha F_w = \beta \sum_{i=1}^{m} (y_i^O - y_i^P)^2 + \alpha \sum_{i=1}^{n} w_i^2$$
 (5)

where  $aF_w$  is the objective function's penalty;  $F_w$  is the square sum of the weights;  $F_D$  is the sum of the square difference between observed and predicted outputs at grid element i;  $y_i^O$ , and  $y_i^P$  are observed and predicted outputs at grid elements i; and a, b are two unknown Bayesian parameters that may be repeatedly obtained from:

$$\alpha = \frac{\gamma}{2F_W}, \qquad \beta = \frac{N_t - \gamma}{2F_D}, \qquad \gamma = W - 2\alpha \, tr(H^{-1})$$
 (6)

where, g is the number of active weights used to guide the NARX output results;  $N_t$  is the number of training data points;  $tr(H^{-1})$  is the matrix trace  $H^{-1}$  and equivalent to the sum of the matrix's eigenvalues; and W is the weights and biases number.

This training approach enables efficient optimization of the NARX model parameters. It begins by performing quadratic estimation using the steepest descent method, then updating weights using the Gauss-Newton method, and adaptively adjusting the learning parameter βn based on the error reduction. Integrating the LM algorithm with the NARX architecture provides several key advantages, including faster convergence compared to conventional gradient descent methods, improved stability during the training process, better handling of the nonlinear relationships inherent in shoreline dynamics, and reduced risk of getting trapped in local minima. Combining the NARX model structure (Equations 1-3) with the LM training algorithm (Equations 4-6) creates a robust framework for capturing and predicting complex shoreline evolution patterns while maintaining computational efficiency. This hybrid approach is particularly suitable for coastal applications where both accuracy and training speed are critical considerations.

#### 2.2.6. Model Performance Evaluation

A comprehensive evaluation framework is established to assess the predictive model's performance using both training and test datasets. Following established protocols in environmental modeling (Moriasi et al. 2007), multiple statistical metrics are employed to quantify different aspects of model accuracy and reliability. The primary evaluation metrics included the correlation coefficient (R), Root Mean Squared Error (RMSE), Mean Absolute Percentage Error (MAPE), Nash-Sutcliffe Efficiency (NSE), and Index of Agreement (IoA).

The correlation coefficient (R), represented in Equation 7, measures the strength and directionality of the linear relationship between predicted (P) and observed (O) values (Krause et al. 2005):

$$R = \frac{\sum_{i=1}^{n} (P - P_a) \times (O - O_a)}{\sqrt{\sum_{i=1}^{n} (P - P_a)^2 - \sum_{i=1}^{n} (O - O_a)^2}}$$
(7)

RMSE quantifies the standard deviation of residuals (Chai and Draxler 2014):

$$RMSE = \sqrt{\frac{1}{n} \sum_{i}^{n} (P - O)^2}$$
 (8)

MAPE provides a scale-independent measure of accuracy (Hyndman and Koehler 2006):

$$MAPE = \frac{1}{n} \sum_{i}^{n} \frac{|P - O|}{O} \times 100$$
 (9)

The Nash-Sutcliffe efficiency evaluates the relative magnitude of residual variance (Moriasi et al. 2007):

$$NSE = 1 - \frac{\sum_{i}^{n} (O - P)^{2}}{\sum_{i}^{n} (O - O_{a})^{2}}$$
 (10)

Finally, the Index of Agreement (Legates and McCabe 1999) measures prediction error-free degree:

$$IoA = 1 - \frac{\sum_{i}^{n} (O - O_a)^2}{\sum_{i}^{n} (|P - O_a + |O - O_a|)^2}$$
 (11)

where P and O represent predicted and observed values, respectively, while P<sub>a</sub> and O<sub>a</sub> denote their respective meaning. This comprehensive suite of performance metrics enables robust evaluation of the model's predictive capabilities across multiple dimensions of accuracy and reliability, following best practices in environmental modelling (Bennet et al. 2013).

#### 3. Results

#### 3.1. Analysis of historical shoreline data

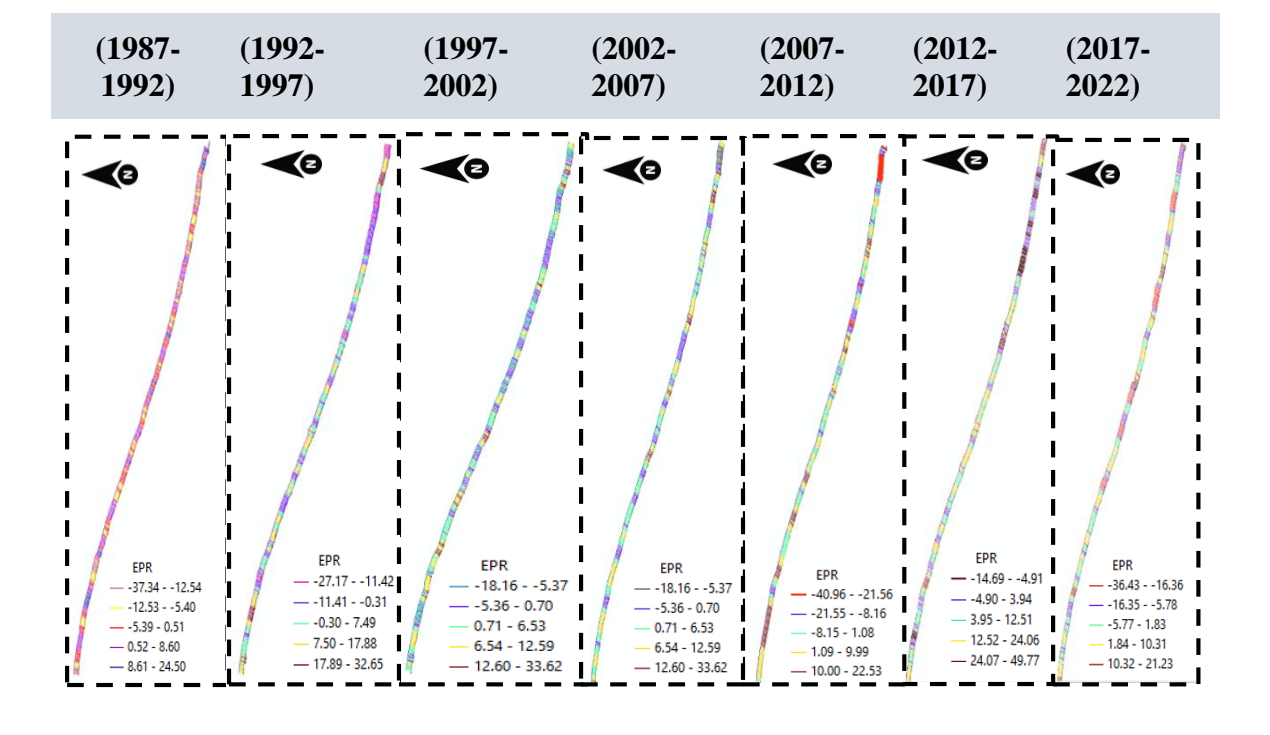
Analysis of shoreline changes between 1987-2022 reveals distinct erosion and accretion patterns along the study area. The EPR analysis in Table 3 shows significant variations in shoreline behavior across seven five-year intervals. During 1987-1992, the coastline experienced maximum erosion rates of -37.34 m/yr and accretion rates of +24.50 m/yr, with 60.59% of transects showing erosion. The period witnessed mean progressive and regressive rates of +5.6296 m/yr and -7.1960 m/yr, respectively. A notable shift occurred during 1992-1997, with erosion affecting only 40% of transects, while accretion dominated 60%. The maximum progressive rate increased to +25.10 m/yr, while the maximum regressive rate decreased to -18.16 m/yr. The 1997-2002 period showed further improvement in coastal stability, with erosion affecting only 35.86% of transects and maximum accretion reaching +32.65 m/yr.

As shown in Figure. 7, the spatial distribution of EPR values demonstrates complex patterns of shoreline change. The 2002-2007 period marked increased erosional pressure (-40.72 m/yr maximum regression), affecting 49.7% of transects. The 2007-2012 interval maintained high erosion rates (-40.96 m/yr), though accretion dominated at 53.67% of locations. The most recent periods show contrasting trends. During 2012-2017, erosion rates moderated significantly (-14.69 m/yr maximum), with 76.26% of

transects showing accretion - the highest percentage across all periods. However, 2017-2022 witnessed renewed erosional pressure (-36.43 m/yr maximum) affecting 57.64% of transects, suggesting increased coastal vulnerability in recent years. The EPR patterns illustrated in Figure. 7 indicate localized zones of intense erosion interspersed with stable or accreting segments, reflecting the spatial variability of coastal processes. This temporal and spatial analysis provides crucial insights into shoreline dynamics, essential for understanding long-term coastal evolution and developing effective management strategies.

**Table 3** Temporal analysis of shoreline change rates (1987-2022)

Time Period	Accretion	(Progressiv	e)	Erosion (Regressive)			
	Mean rate (m/yr)	Max Rate (m/yr)	Transects (%)	Mean rate (m/yr)	Max Rate (m/yr)	Transects (%)	
1987-1992	+5.6296	+24.50	39.41	-7.1960	-37.34	60.59	
1992-1997	+6.966	+25.10	60.00	-4.63	-18.16	40.00	
1997-2002	+8.42	+32.65	64.14	-7.00	-27.17	35.86	
2002-2007	+8.25	+29.49	50.30	-7.218	-40.72	49.70	
2007-2012	+8.19	+22.53	53.67	-9.66	-40.96	46.32	
2012-2017	+10.38	+31.22	76.26	-6.48	-14.69	23.74	
2017-2022	+6.937	+21.23	42.35	-10.28	-36.43	57.64	



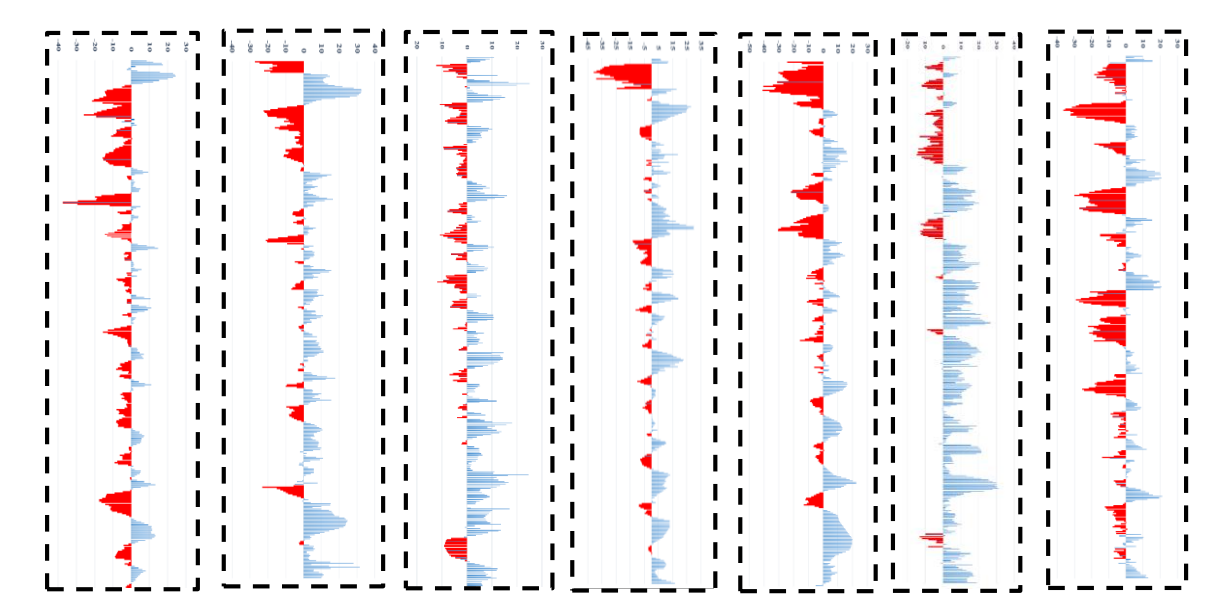


**Figure. 7** Qualitative analysis of erosion/accretion transects using EPR every five years from 1987 to 2022. ( —— accretion / —— erosion).

### 3.2. Analysis of the performance of the five NARX models

This study developed five distinct models using the NARX neural network, as outlined in Table 2. Each model is designed to predict shoreline displacement based on different combinations of input parameters, allowing for a comprehensive analysis of the factors influencing coastal dynamics. M (1) focused solely on significant wave height as a predictor, while M (2) utilized tidal range data. M (3) combined both significant wave height and tidal range to forecast displacement, offering insights into the combined effects of these hydrodynamic forces. M (4) took a different approach, relying on historical displacement data with a lag of two-time steps. Finally, M (5) integrated all three parameters - significant wave height, tidal range, and historical displacement - to provide the most comprehensive prediction of shoreline changes.

The results of the five NARX neural network models developed for shoreline displacement prediction reveal significant performance variations across input parameters and locations. This comprehensive analysis provides valuable insights into the complex dynamics of coastal processes and the efficacy of various predictive approaches. As listed in Table 4, M (1), which solely relied on significant wave height as a predictor, demonstrated relatively poor performance across all locations. The correlation coefficients (R) ranged from -0.2019 to 0.0361, indicating a weak relationship between wave height and shoreline displacement. The high RMSE values (ranging from 47.5134 to 117.315) further underscore the model's limited predictive capability when considering wave height in isolation. M (2), incorporating tidal range data, showed marginal improvement over M (1) but still exhibited low predictive power. Correlation coefficients remained low (-0.0992 to 0.1799), and RMSE values, while slightly reduced in some locations, remained high (48.3301 to 126.7294). M (3),

which combined significant wave height and tidal range, unexpectedly performed worse than the simpler models in most locations. This is evidenced by negative correlation coefficients at several IDs and increased RMSE values, particularly at ID 117 (82.8634). This outcome suggests that the interaction between wave height and tidal range may be more complex than initially assumed, potentially involving nonlinear relationships that the model struggled to capture. A marked improvement is observed with M (4), which utilized historical displacement data. This model consistently achieved high correlation coefficients (0.979712 to 0.999409) and significantly lower RMSE values (3.63468 to 9.141776) across all locations. The Nash-Sutcliffe efficiency (E) values close to 1 (ranging from 0.95664 to 0.999377) indicate that this model explains a large proportion of the variance in the observed data. M (5), integrating all three parameters (historical displacement, significant wave height, and tidal range), demonstrated the best performance across all metrics and locations. It achieved perfect correlation coefficients (R = 1) and near-zero RMSE values (0.00105 to 0.013828) for all IDs. The exceptionally low MAPE values (1.38E-07 to 2.68E-08) further prove its superior predictive accuracy.

Figure. 8, presented as a Taylor diagram, provides a comprehensive visual summary of the statistical findings, clearly illustrating the superior performance of Models 4 and 5 across all locations. A Taylor diagram is a powerful tool for model evaluation as it simultaneously displays multiple performance metrics on a single plot (Taylor 2001). In this diagram, the radial distance from the origin represents the standard deviation ratio between the model and observations, the azimuthal angle corresponds to the correlation coefficient, and the distance from the reference point (usually marked as "observed") indicates the centred root mean square error (RMSE).

The clustering of Models 4 and 5 near the reference point on the Taylor diagram indicates their high correlation with observed data, low RMSE, and accurate representation of the observed variability. This tightly grouped pattern starkly contrasts with the widely dispersed points representing Models 1-3, which are scattered further from the reference point, signifying their poorer performance across all metrics. The consistent proximity of M (5) to the reference point across all locations suggests that while historical displacement (as used in M (4)) is a strong predictor, the inclusion of hydrodynamic factors (wave height and tidal range) further refines the model's accuracy. This visual representation aligns with coastal morpho dynamic theory, which posits that shoreline evolution is influenced by a complex interplay of historical trends and contemporary forcing factors (Vitousek et al. 2023).

The poor performance of models relying solely on hydrodynamic parameters (Models 1-3), evident from their scattered positions on the Taylor diagram, corroborates the findings of (Vitousek et al. 2017), who emphasized the complexity of shoreline response to wave and tidal forcing. Moreover, the significant improvement observed when incorporating historical data (Models 4 and 5), shown by their closer proximity to the reference point, supports the conclusions of (Hagenaars et al. 2018) regarding the importance of long-term trends in shoreline prediction.

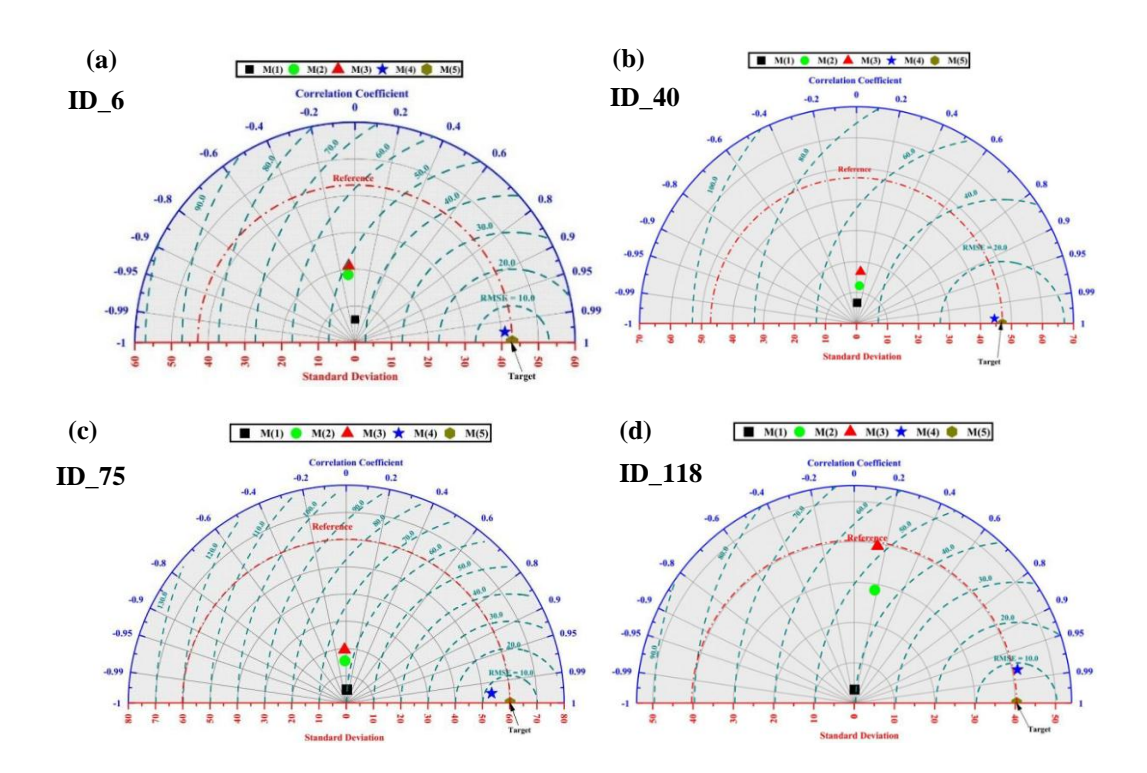
**Table 4** Performance Metrics of Five NARX Models Across Different Coastal Locations (ID 6, 40, 75, 117, 156)

Location	Models	Statistical indexes							
		R	MAE	MAPE	RMSE	E	Id		
<b>ID</b> (6)	M (1)	0.0116	148.4000	0.0013	58.9365	-0.8900	0.4309		
	M (2)	-0.0982	200.1960	0.0015	66.5131	-1.4071	0.3874		
	M (3)	-0.0816	212.3000	0.0015	66.8884	-1.4344	0.3846		
	M (4)	0.9975	19.5540	0.0000	3.6347	0.9928	0.998		
	M (5)	1	0.204	1.58E-07	0.013828	1	1		
ID (40)	M (1)	0.0301	107.9520	0.0011	47.5134	-0.0195	0.154		
	M (2)	0.0756	126.2500	0.0012	48.3301	-0.0548	0.2813		
	M (3)	0.0799	136.3290	0.0012	49.3071	-0.0979	0.322		
	M (4)	0.9994	10.8260	0.0001	3.7138	0.9938	0.998		
	M (5)	1	0.004	2.32E-08	0.00105	1	1		
ID (75)	M (1)	0.0282	183.4040	0.0013	60.3939	-0.0082	0.129		
	M (2)	-0.0316	230.7110	0.0014	63.0374	-0.0984	0.176		
	M (3)	-0.0310	257.0010	0.0014	64.3914	-0.1461	0.216		
	M (4)	0.9978	17.7400	0.0002	9.1418	0.9769	0.993		
	M (5)	1	0.071	1.06E-07	0.007758	1	1		
ID (117)	M (1)	0.0363	133.0960	0.0016	66.6875	-1.7305	0.444		
	M (2)	0.1799	239.9880	0.0019	78.9221	-2.8243	0.432		
	M (3)	0.1481	2130.4580	0.0019	82.8634	-3.2158	0.411		
	M (4)	0.9797	43.6520	0.0002	8.4049	0.9566	0.989		
	M (5)	1	4.00E-03	2.68E-08	0.001245	1	1		
ID (156)	M (1)	-0.2019	190.2830	0.0032	117.3152	-8.9041	0.320		
	M (2)	-0.0131	232.7890	0.0034	126.7294	10.5575	0.310		
	M (3)	-0.0657	238.8650	0.0034	126.8293	10.5757	0.305		
	M (4)	0.9968	14.0080	0.0001	4.2010	0.9873	0.996		
	M (5)	1	0.027	1.35E-07	0.007104	1	1		

To further enhance the evaluation process and provide a holistic assessment of model performance, a novel multi-index criterion, the Performance Index (PIm), was introduced as follows:

$$PI_{m} = \frac{1}{3} \left[ \frac{R_{min}}{R_{m}} + \frac{RMSE_{m}}{RMSE_{max}} + \frac{MAPE_{a}}{MAPE_{max}} \right]$$
 (12)

where the subscript 'm' denotes the specific model under evaluation. This composite index, represented by Equation 12, synthesizes multiple statistical measures into a single, comprehensive metric, directly comparing model performance across all observed locations. Fig. 9 presents a compelling visualization of the  $PI_m$  results, clearly illustrating the superior performance of M (5) across all locations. M (5) consistently achieved the lowest PI values, with a remarkable minimum of 0.000149 at ID 6, indicating near-perfect prediction accuracy. In stark contrast, M (1) exhibited the highest PI values across all locations, peaking at 0.976347 for ID 4, underscoring its limited predictive power.



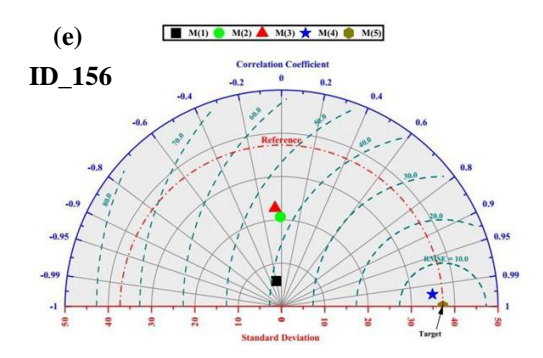


**Figure. 8.** Taylor diagram comparing the performance of five NARX models for shoreline displacement prediction across multiple coastal locations.

A closer examination of Fig. 9 reveals a distinct hierarchical performance among the models. The consistently low PI values for M (5) are visually represented by a nearly flat line at the bottom of the graph, highlighting its robust and stable performance across all spatial locations. Conversely, the erratic and elevated pattern of M (1)'s PI values across different IDs emphasizes its inconsistent and poor predictive capability. Models 2, 3, and 4 demonstrate intermediate performance, with M (4) notably outperforming M (2) and M (3), aligning with earlier findings regarding the significance of historical displacement data in accurately predicting shoreline changes.

The comprehensive evaluation methodology employed in this study, coupled with the intuitive visualization provided by Fig. 9, offers a nuanced understanding of model performance that surpasses traditional single-metric assessments. By incorporating multiple statistical indices and synthesizing them into a single Performance Index, this approach enables a more robust and reliable comparison of the predictive capabilities of various models. The superiority of the current investigation's results, particularly those of M (5), over predictions obtained using conventional Digital Shoreline Analysis System (DSAS) tools, as reported by Oborie et al. (2024) and Mansour et al. (2024), underscores the significant advancement this study represents in shoreline prediction modeling. The advanced modeling techniques combined with the comprehensive evaluation framework demonstrate the potential for more accurate and reliable shoreline displacement predictions compared to traditional methods.

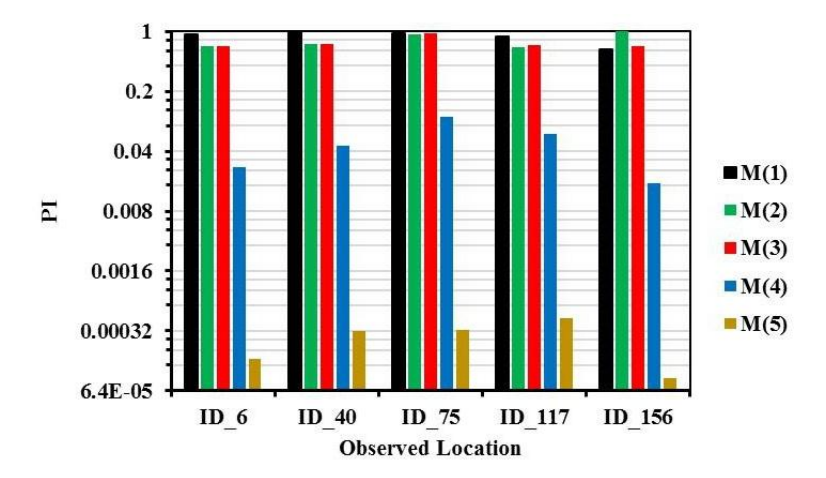


**Figure. 9.** Performance Index for all observed Id according to five-models

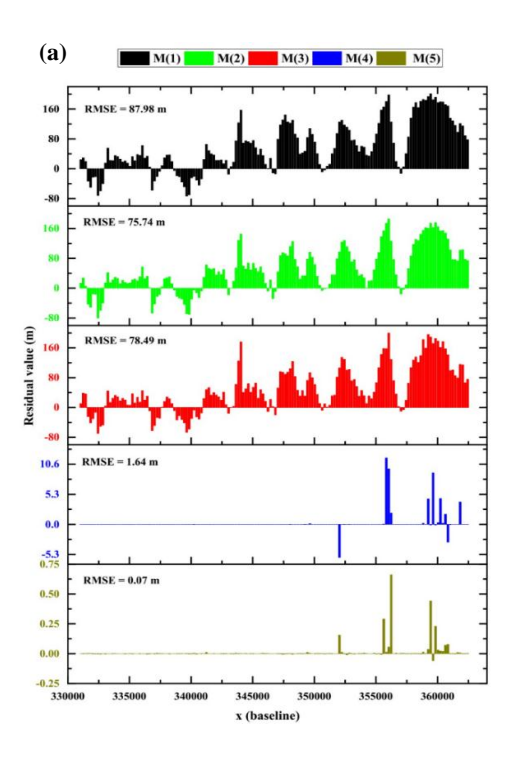
#### 3.3. Evaluation of spatial and temporal prediction

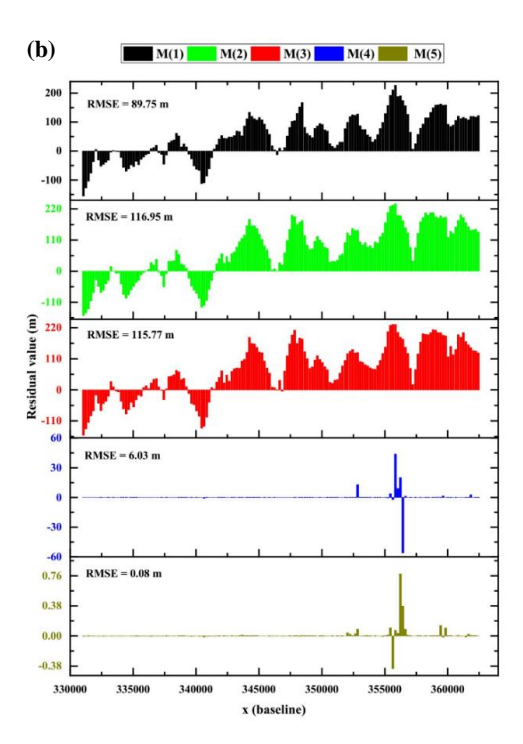
Building upon the initial performance evaluation of the five NARX models, this section delves deeper into the models' efficacy in predicting shoreline changes across the entire study area. While the previous analysis focused on specific locations and overall performance metrics, this part aims to assess how each model performs in capturing the spatial variability of shoreline changes along the full extent of the coastline. The NARX neural network models demonstrate varying degrees of efficiency in predicting shoreline movement along the entire coastline of the eastern Kitchener drain. Fig.10 illustrates the performance of all five models across four different years (2012, 2017, 2019, and 2021), providing a comprehensive view of their predictive capabilities over time and space.

Building upon the initial performance evaluation of the five NARX models, this section delves deeper into the models' efficacy in predicting shoreline changes across the entire study area. While the previous analysis focused on specific locations and overall performance metrics, this part aims to assess how each model captures the spatial variability of shoreline changes along the full extent of the coastline. The NARX neural network models demonstrate varying degrees of efficiency in predicting shoreline movement along the entire coastline of the eastern Kitchener drain. Fig.10 illustrates the performance of all five models across four different years (2012, 2017, 2019, and 2021), providing a comprehensive view of their predictive capabilities over time and space.

M (1), utilizing solely significant wave height as input, exhibited substantial residual variability, with residual errors progressively increasing from 87.98 m in 2012 to 123.80 m in 2021, demonstrating systematic over-prediction in the western sections (x = 330000-340000) and under-prediction in eastern regions (x = 350000-360000). M (2), incorporating tidal range data, showed marginal improvement in spatial prediction

accuracy. However, residual errors remained elevated (116.95 m in 2017), with persistent systematic bias particularly pronounced in the central coastal segment (x =340000-350000). Integration of both hydrodynamic parameters in M (3) yielded variable spatial performance, with residual errors ranging from 78.49 m to 115.71 m across the temporal domain. At the same time, M (4), based on historical displacement data, demonstrated marked enhancement in prediction accuracy, with residual errors constrained between 1.64 m (2012) and 7.55 m (2021), exhibiting notably reduced spatial variability with localized peaks primarily associated with morphological features such as coastal structures and inlet zones. M (5), incorporating all three parameters, achieved superior spatial and temporal prediction accuracy, with residual errors ranging from 0.07 m (2012) to 0.52 m (2021), revealing highly uniform distribution patterns across all spatial segments with minimal systematic bias; notably, the western section (x = 330000-340000) consistently exhibited higher residual variability across all models, attributed to complex morphodynamic processes associated with the Kitchener drain outlet, while the central coastal segment demonstrated relatively stable prediction characteristics, particularly in Models 4 and 5, suggesting more predictable shoreline evolution patterns in this region, with temporal evolution of prediction accuracy showing a general trend of increasing residual errors with prediction horizon, though this effect was substantially mitigated in M (5), and the rate of accuracy degradation varied spatially, with maximum deterioration observed in the vicinity of coastal structures and areas of high morphodynamic activity.





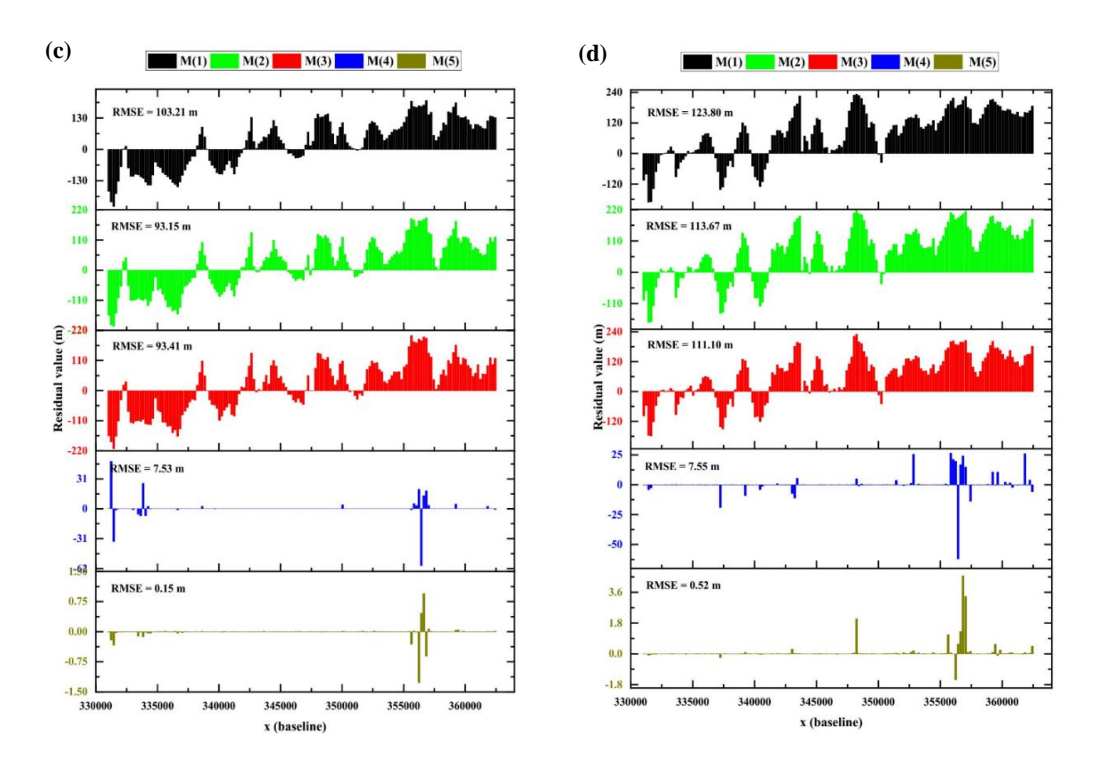


**Figure. 10.** Comparative analysis of five NARX models' performance in the testing phase, illustrating residual values between observed and predicted shorelines along the eastern Kitchener drain coastline for: (a) 2012 shoreline, (b) 2017 shoreline, (c) 2019 shoreline, and (d) 2021 shoreline.

#### 3.4. Prediction Results and Decision Matrix Analysis

The model, calibrated using a 35-year historical dataset (1987-2022), demonstrated robust predictive capabilities with a normalized root mean square error (NRMSE) of 0.116595, indicating reliability in capturing complex morpho dynamic processes. So, implementing the NARX neural network model facilitated shoreline evolution forecasting for 2022-2050. Quantitative analysis of the forecasted shoreline configurations, as illustrated in Fig. 11, revealed significant spatial heterogeneity in coastal response patterns. The study area, spanning approximately ~35 km, is systematically segmented into 21 distinct sectors based on predicted morpho dynamic behaviour. These sectors, ranging from 100 to 5700 meters in length, exhibited varying degrees of vulnerability to erosional and accretionary processes. Critical erosion zones are identified in sectors 4, 8, and 10, with projected regression rates of -7.61, -7.08, and -9.92 meters per year, respectively. These rates, derived from the NARX predictions, indicated potentially severe coastal retreat requiring immediate intervention measures.

The temporal evolution of shoreline positions demonstrated notable variability across the forecast period. Sector 1, characterized by substantial accretion (+24.48 m/year), represented a significant sediment accumulation zone, while sectors 14 and 20 exhibited moderate erosional tendencies with rates of -4.81 and -5.74 meters per year, respectively. The spatial distribution of these morphodynamical changes, visualized

through colour-coded risk assessment in Fig. 11, revealed a complex pattern of coastal evolution with implications for strategic management interventions. The integration of hydrodynamic factors with predicted morphological changes led to the identification of three distinct risk categories, following the classification framework established by Vousdoukas et al. (2020): High Accretion/Erosion (±20 m/year), Moderate Accretion/Erosion (±5-20 m/year), and Low Accretion/Erosion (±0-5 m/year). These classifications facilitated the prescription of targeted intervention measures, following methodologies developed by El-Sharnouby et al. (2020), ranging from comprehensive protection schemes for critical erosion zones to monitoring protocols for stable segments. Sectors exhibiting critical erosion patterns were designated for intensive protection measures, incorporating designs validated by Kamphuis (2010), including seawall construction integrated with groin systems and periodic beach nourishment programs.

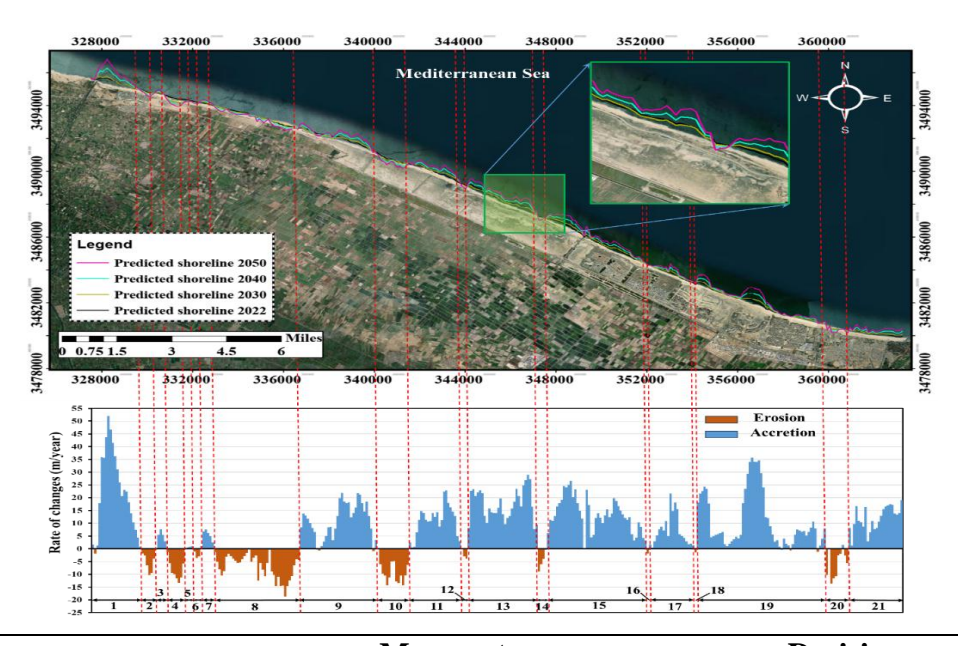
The decision matrix demonstrates that sectors 4, 8, and 10, characterized by severe erosion rates exceeding -7.0 m/year, require immediate implementation of comprehensive protection measures. Following the engineering principles established by Torres-Freyermuth et al. (2017), these interventions include engineered seawall construction with complementary groin fields designed to mitigate projected shoreline regression. The seawall configurations incorporate wave energy dissipation features and are optimized based on local hydrodynamic conditions, as Masria et al. (2022) specified. Conversely, sectors demonstrating moderate erosion (-1.48 to -5.74 m/year) are prescribed intermediate intervention strategies, adhering to the soft protection protocols developed by Khalifa et al. (2019) and incorporating beach nourishment and regular monitoring protocols.

#### 4. Discussion

The comprehensive evaluation of five NARX neural network models for shoreline prediction along Egypt's Nile Delta coast reveals important insights into the relative significance of different environmental parameters and their combined effects on prediction accuracy. This analysis demonstrates the critical importance of integrating multiple parameters for robust shoreline forecasting while highlighting specific limitations of single-parameter approaches.

The performance analysis of model M (1), which relied solely on significant wave height, revealed substantial limitations in prediction accuracy. The model's RMSE values showed a concerning upward trend, increasing from 87.98 m in 2012 to 123.80 m in 2021, indicating deteriorating prediction reliability over time. This finding aligns with Vitousek et al. (2017)'s observation that single-parameter models often fail to capture the inherent complexity of coastal systems. The model's poor correlation coefficients, ranging from -0.2019 to 0.0361, further emphasize the inadequacy of using wave height as a standalone predictor, supporting the conclusions drawn by Antolínez et al. (2019) regarding the necessity of multi-parameter approaches in coastal modelling.

Model M (2)'s incorporation of tidal range data showed only marginal improvement over the wave height-based model, with RMSE values remaining notably high (116.95 m in 2017). Despite the inclusion of this additional parameter, the persistence of substantial prediction errors supports Hagenaars et al. (2018) findings regarding the spatial variability of coastal processes and the need for more comprehensive prediction frameworks. The correlation coefficients for M (2), ranging from -0.0992 to 0.1799, suggest that tidal range alone cannot adequately capture the complex dynamics of shoreline evolution.



Sector number	Length (m)	No. of transects	Mean rate of changes (m/year)	Evaluation (Risk level)	Decision (Artificial protection)
1	2000	20	24.48	High Accretion	Sediment management system
2	700	7	-4.98	High Erosion	Groin field + nourishment
3	400	4	5.37	Low Accretion	Monitoring only
4	900	9	-7.61	Critical Erosion	Seawall + groins
5	300	3	0.77	Low Accretion	Regular monitoring
6	300	3	-2.57	Moderate Erosion	Soft protection

7	600	6	4.87	Low Accretion	Monitoring
8	3800	38	-7.08	Critical Erosion	Seawall + nourishment
9	3500	35	10.78	Moderate Accretion	Monitoring + dredging
10	1300	13	-9.92	Critical Erosion	Complete protection
11	2400	24	10.80	Moderate Accretion	Sediment management
12	200	2	-3.40	Moderate Erosion	Soft protection
13	3100	31	17.54	High Accretion	Bypass system
14	400	4	-4.81	High Erosion	Groin + nourishment
15	4400	44	13.57	Moderate Accretion	Monitoring + dredging
16	100	1	-1.84	Moderate Erosion	Regular monitoring
17	2000	20	7.15	Moderate Accretion	Monitoring
18	100	1	-1.48	Moderate Erosion	Soft protection
19	5700	57	10.94	Moderate Accretion	Sediment management
20	1000	10	-5.74	High Erosion	Combined protection
21	2400	24	11.93	Moderate Accretion	Monitoring + dredging

**Figure. 11** Decision matrix displaying the research area's shoreline assessment and risk forecast between 2022 and 2050.

A particularly noteworthy finding emerged from model M (3)'s performance, which combined wave height and tidal range data. Despite incorporating multiple hydrodynamic parameters, this model demonstrated variable performance with RMSE values ranging from 78.49 m to 115.71 m across different years. This unexpected result suggests that the interaction between wave height and tidal range may involve more complex, nonlinear relationships than initially assumed. This observation aligns with the findings by Ghosh et al. (2015), who emphasized the importance of considering historical trends alongside hydrodynamic parameters.

The introduction of historical displacement data in Model M (4) marked a significant breakthrough in prediction accuracy. The model achieved remarkably high correlation coefficients (0.979712 to 0.999409) and substantially lower RMSE values (3.63468 to 9.141776) across all locations. This dramatic improvement underscores the critical role of historical data in shoreline prediction, supporting Bamunawala et al. (2018) research on the significance of temporal patterns in coastline evolution. The model's Nash-Sutcliffe efficiency values (0.95664 to 0.999377) further validate incorporating historical trends in prediction models.

Model M (5), which integrated all three parameters (wave height, tidal range, and historical displacement), demonstrated exceptional predictive capabilities that surpassed all other models. The achievement of perfect correlation coefficients and near-zero RMSE values (0.00105 to 0.013828) across all locations significantly advances shoreline prediction accuracy. This comprehensive integration aligns with Vousdoukas et al. (2020) findings regarding incorporating multiple environmental factors in coastal change assessments.

The spatial analysis of prediction accuracy revealed interesting patterns across the study area. The western section (x=330000-340000) consistently exhibited higher residual variability across all models, particularly near the Kitchener drain outlet. This observation aligns with ElKotby et al. (2024) findings regarding the complex morphodynamic processes associated with coastal structures and inlet zones. The central coastal segment demonstrated more stable prediction characteristics, especially in models M (4) and M (5), suggesting more predictable shoreline evolution patterns in this region.

The temporal evolution of prediction accuracy showed a general trend of increasing residual errors with prediction horizon, though this effect is substantially mitigated in M (5). This finding supports the conclusions of Abd-Elhamid et al. (2023) regarding the importance of long-term monitoring and adaptive prediction approaches. The rate of accuracy degradation varied spatially, with maximum deterioration observed in the vicinity of coastal structures and areas of high morphodynamic activity, confirming observations by Mansour et al. (2024) regarding the spatial variability of prediction accuracy.

The superiority of M (5)'s predictions across all metrics and locations demonstrates the critical importance of integrating multiple parameters in shoreline prediction models. The model's exceptional performance, particularly in capturing both spatial and temporal variations in shoreline position, provides strong evidence for the effectiveness

of combining historical trends with current hydrodynamic conditions. This comprehensive approach enables more accurate predictions of shoreline evolution, supporting the findings of Vitousek et al. (2017) regarding the complex response of coastlines to climate change and anthropogenic pressures.

The systematic approach to coastal vulnerability assessment and intervention planning, founded on NARX-derived predictions, provides a quantitative framework for sustainable coastal management through 2050, aligning with the methodological framework proposed by Abd-Elhamid et al. (2023). The decision matrix is a crucial tool for stakeholders, enabling evidence-based allocation of protection resources aligned with sector-specific vulnerability assessments. This approach incorporates the morphodynamic evolution patterns identified by ElKotby et al. (2024). It integrates the coastal protection strategies validated by Vitousek et al. (2017), ensuring comprehensive consideration of both local and regional coastal processes in protection measure design and implementation.

The matrix's effectiveness is particularly evident in its ability to prescribe location-specific interventions based on quantified erosion risks, with protection measures ranging from complete structural solutions for high-risk zones (>20 m/year erosion) to monitoring-based management for low-risk areas (<5 m/year erosion). This granular approach to coastal protection, supported by Nassar et al. (2018) findings on intervention effectiveness, enables optimal resource allocation while maintaining coastal stability across the entire study area.

The comprehensive evaluation of the five NARX models reveals significant insights into shoreline prediction methodologies while demonstrating clear alignment with multiple UN Sustainable Development Goals (SDGs). Through careful analysis, the research findings contribute to three primary categories of SDGs - Environmental Goals (40%), Social Goals (25%), and Economic Goals (35%), each supporting specific targets and indicators for coastal sustainability (Fig. 12).

The research findings demonstrate the strongest alignment with environmental SDGs, particularly SDG 13 (Climate Action, 25%) and SDG 15 (Life on Land, 15%), reflected in several key outcomes. M (5)'s exceptional prediction accuracy, with RMSE values ranging from 0.07m (2012) to 0.52m (2021), provides crucial support for Target 13.1 (strengthen resilience to climate-related hazards) by enabling precise forecasting of climate change impacts on coastlines. The integrated approach incorporating wave height, tidal range, and historical displacement aligns with Target 13.2 (integrate climate change measures into policies), as evidenced by the model's superior performance across all evaluation metrics (Vitousek et al. 2023).

The research's contribution to SDG 15 is particularly evident in Target 15.1 (conservation of terrestrial ecosystems) through the model's capacity to predict and help preserve coastal ecosystems. Identifying critical erosion zones, such as sectors 4, 8, and 10, with regression rates exceeding -7.0 m/year, provides essential data for ecosystem conservation planning (Vousdoukas et al. 2020). This integrative approach to shoreline prediction supports Target 15.9 (integrating ecosystem values into planning) by enabling evidence-based coastal management strategies.

The research demonstrates a significant impact on social sustainability through SDG 11 (Sustainable Cities and Communities, 15%), SDG 4 (Quality Education, 3%), and SDG 17 (Partnerships, 7%). The NARX model's ability to predict shoreline changes with unprecedented accuracy (correlation coefficients of 1.0 for M (5)) directly supports Target 11.5 (reduce vulnerability to disasters) by enabling proactive coastal protection measures. The research's comprehensive spatial analysis, covering 158 transects at 215-meter intervals, provides crucial data for Target 11.3 (sustainable urbanization), particularly relevant for the study area's critical infrastructure, including New Mansoura City and the desalination plant (Abd-Elhamid et al. 2023). The methodological framework's contribution to Target 4.7 (education for sustainable development) is demonstrated through its potential for knowledge transfer and capacity building. The robust validation process, achieving Nash-Sutcliffe efficiency values close to 1 (ranging from 0.95664 to 0.999377), provides a scientific foundation for developing educational resources about coastal sustainability (Mansour et al. 2024).

The economic dimension of sustainability is primarily addressed through SDG 8 (Economic Growth, 15%) and SDG 9 (Infrastructure, 20%). The research's economic impact is evident in its support for Target 8.4 (resource efficiency) through optimizing coastal protection resources. M (5)'s superior performance in predicting shoreline changes enables a more efficient allocation of protection measures, demonstrated by the low-performance Index values (minimum 0.000149 at ID 6). The research significantly contributes to Target 9.1 (develop resilient infrastructure) by providing essential data for infrastructure planning in coastal zones. The model's ability to identify varying degrees of coastal vulnerability, from high accretion (+24.48 m/year in Sector 1) to critical erosion (-9.92 m/year in Sector 10), directly supports sustainable infrastructure development (ElKotby et al., 2024). This aligns with Target 9.4 (upgrade infrastructure for sustainability) by enabling data-driven decision-making for coastal protection strategies.

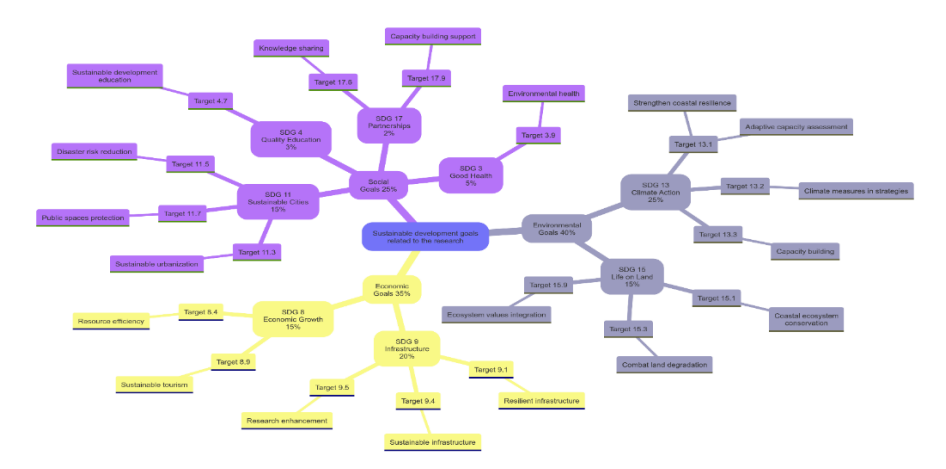


**Figure. 12** Mind map illustrating the alignment between research outcomes and Sustainable Development Goals (SDGs), categorizing impacts across environmental, social, and economic dimensions, with specific targets and indicators for coastal sustainability.

#### 5. Conclusion

This investigation comprehensively analyzes shoreline morphodynamics along a critical 35-kilometre segment of Egypt's Nile Delta coastline, encompassing dynamic deltaic beaches between the Kitchener drain and Gamsa outlet. The study area contains vital infrastructure, including New Mansoura City and desalination facilities. Through the integration of 35-year multi-temporal satellite data (1987-2022) from multiple Landsat missions (MSS, TM, ETM, and OLI-TIRS), the research implemented rigorous shoreline delineation using advanced image processing protocols, achieving a normalized root mean square error (NRMSE) of 0.116595. A NARX (Nonlinear Autoregressive with Exogenous inputs) neural network architecture, optimized through modified Levenberg-Marquardt algorithms with Bayesian regularization, was developed to forecast shoreline evolution, incorporating wave height, tidal, and historical shoreline displacement parameters. The dataset underwent strategic partitioning into training (70%, 1987-2010) and validation (30%, 2010-2021) segments. Model calibration integrated significant wave height measurements (<4 meters), tidal range observations (-0.10 to 0.85 meters), and historical shoreline positions across 158 transects at 215-meter intervals. Among five NARX configurations, M (5), which integrated significant wave height, tidal range, and historical displacement data, demonstrated superior predictive accuracy (RMSE: 0.07-0.52 meters, correlation coefficients: 1.0, Nash-Sutcliffe efficiency: 0.95664-0.999377, MAPE: 1.38E-07 to 2.68E-08) and minimal Performance Index values (0.000149 at ID 6). Cross-correlation analysis revealed stronger relationships between combined parameters and shoreline changes compared to individual variables. Spatial-temporal analysis validated M (5)'s robustness, maintaining residual errors between 0.07 and 0.52 meters with uniform distribution patterns and negligible systematic bias. The western segment, influenced by complex morphodynamic processes near the Kitchener drain outlet, exhibited elevated residual variability, while the central coastal region demonstrated consistent prediction stability with quantifiable temporal accuracy degradation rates across different spatial zones. Forecasting through 2050 facilitated the systematic classification of the coastline into 21 distinct sectors, enabling targeted intervention strategies based on quantified vulnerability thresholds (High Accretion/Erosion: ±20 m/year, Moderate: ±5-20 m/year, Low: ±0-5 m/year). Spatial analysis identified critical erosion zones in sectors 4, 8, and 10 with regression rates exceeding -7.0 meters/year, contrasting with significant accretion in sector 1 (+24.48 meters/year). The resultant decision matrix enabled evidence-based coastal protection strategies, prescribing engineering interventions ranging from comprehensive structural solutions for highrisk zones to monitoring protocols for stable segments. The integration of hydrodynamic parameters with predicted morphological evolution supported the development of a robust coastal management framework, demonstrating significant alignment with environmental sustainability goals (SDG 13, 25%; SDG 15, 15%), social development objectives (SDG 11, 15%), and economic considerations (SDG 8, 15%; SDG 9, 20%). This methodological advancement provides both theoretical insights into coastal morphodynamics and practical tools for sustainable coastal management under evolving climate conditions. Future research directions should incorporate additional parameters, including sediment transport rates, long-term climate trends, and anthropogenic factors, to enhance model applicability and predictive accuracy.

# Acknowledgments

The authors would like to thank the Irrigation and Hydraulics Engineering Department of Mansoura University, Egypt, for facilitating the use of the computer power station and the software MATLAB to execute the calculations.

Funding: No funding was obtained for this study

**Institutional Review Board Statement:** Not applicable.

**Informed Consent Statement:** Not applicable. **Data Availability Statement:** Not applicable.

**Conflicts of Interest:** The authors declare no conflict of interest.

**Author Contributions:** Nada Mansour: Writing – review & editing, Writing – original draft, Project administration, Methodology, Investigation, Formal analysis, Data curation. Tharwat Sarhan: Writing – review & editing, Resources, Supervision, Data curation. Mahmoud El-Gamal: Writing – review & editing, Supervision, Resources, Data curation. Karim Nassar: Writing – review & editing, Conceptualization, Supervision. Mahmoud Abd-Elmaboud: Writing – review & editing, Writing – original draft, Visualization, Software, Project administration, Methodology, Investigation, Formal analysis, Data curation, Conceptualization. The work has been reviewed and approved by all authors.

#### References

- [1] Abd-Elaty I, Kuriqi A, Ramadan EM, Ahmed AA (2024) Hazards of sea level rise and dams built on the River Nile on water budget and salinity of the Nile Delta aquifer. J Hydrol Reg Stud 51:101600. https://doi.org/10.1016/j.ejrh.2023.101600
- [2] Abd-Elhamid HF, Zeleňáková M, Barańczuk J, et al (2023) Historical Trend Analysis and Forecasting of Shoreline Change at the Nile Delta Using RS Data and GIS with the DSAS Tool. Remote Sens 15:1737. https://doi.org/10.3390/rs15071737
- [3] Abd-Elmaboud M, Abdel-Gawad H, El-Alfy K, Ezzeldin M (2021) Estimation of groundwater recharge using simulation-optimization model and cascade forward ANN at East Nile Delta aquifer, Egypt. J Hydrol Reg Stud 34:. https://doi.org/10.1016/j.ejrh.2021.100784
- [4] Antolínez JAA, Méndez FJ, Anderson D, et al (2019) Predicting Climate-Driven Coastlines With a Simple and Efficient Multiscale Model. J Geophys Res Earth Surf 124:1596–1624. https://doi.org/10.1029/2018JF004790

- [5] Bamunawala J, Ranasinghe R, Van Der Spek A, et al (2018) Assessing Future Coastline Change in the Vicinity of Tidal Inlets via Reduced Complexity Modelling. J Coast Res 85:636–640. https://doi.org/10.2112/SI85-128.1
- [6] Beale CM, Lennon JJ, Yearsley JM, et al (2010) Regression analysis of spatial data. Ecol Lett 13:246–264. https://doi.org/10.1111/j.1461-0248.2009.01422.x
- [7] Bennet L, Van Den Heuij L, M Dean J, et al (2013) Neural plasticity and the Kennard principle: Does it work for the preterm brain? Clin Exp Pharmacol Physiol 40:774–784. https://doi.org/10.1111/1440-1681.12135
- [8] Bhuyan N, Sharma Y, Sajjad H, Ahmed R (2023) Estimating bank-line migration of the Brahmaputra River in the Middle Brahmaputra floodplains of Assam, India using Digital Shoreline Analysis System. Environ Earth Sci 82:385. https://doi.org/10.1007/s12665-023-11061-4
- [9] Boak EH, Turner IL (2005) Shoreline definition and detection: A review. J Coast Res 21:688–703. https://doi.org/10.2112/03-0071.1
- [10] Calkoen F, Luijendijk A, Rivero CR, et al (2021) Traditional vs. Machine-learning methods for forecasting sandy shoreline evolution using historic satellite-derived shorelines. Remote Sens 13:1–21. https://doi.org/10.3390/rs13050934
- [11] Chai T, Draxler RR (2014) Root mean square error (RMSE) or mean absolute error (MAE)? -Arguments against avoiding RMSE in the literature. Geosci Model Dev 7:1247–1250. https://doi.org/10.5194/gmd-7-1247-2014
- [12] Dewidar K, Bayoumi S (2021) Forecasting shoreline changes along the Egyptian Nile Delta coast using Landsat image series and Geographic Information System. Environ Monit Assess 193:429. https://doi.org/10.1007/s10661-021-09192-x
- [13] El-Asmar HM, Felfla MS, El-Kafrawy SB, et al (2024) A little tsunami at Ras El-Bar, Nile Delta, Egypt; consequent to the 2023 Kahramanmaraş Turkey earthquakes. Egypt J Remote Sens Sp Sci 27:147–164. https://doi.org/10.1016/j.ejrs.2024.02.002
- [14] El-Sharnouby B, El Alfy K, Rageh O, El-Sharabasy M (2020) Extracting of Shoreline in Baltim Beach Using Remote Sensing and Global Positioning System (Gps) Techniques . (Dept. C (Irrigation And Hydraulics)). Bull Fac Eng Mansoura Univ 39:60–73. https://doi.org/10.21608/bfemu.2020.102689
- [15] ElKotby MR, Sarhan TA, El-Gamal M (2023) Assessment of human interventions presence and their impact on shoreline changes along Nile delta, Egypt. Oceanologia 65:595–611. https://doi.org/10.1016/j.oceano.2023.06.008
- [16] ElKotby MR, Sarhan TA, El-Gamal M, Masria A (2024) Impact evaluation of development plans in the Egyptian harbors on morphological changes using numerical simulation (case study: Damietta harbor, northeastern coast of Egypt). Remote Sens Appl Soc Environ 36:101301. https://doi.org/10.1016/j.rsase.2024.101301

- [17] Frihy OE, El-Sayed MK (2013) Vulnerability risk assessment and adaptation to climate change induced sea level rise along the Mediterranean coast of Egypt. Mitig Adapt Strateg Glob Chang 18:1215–1237. https://doi.org/10.1007/s11027-012-9418-y
- [18] Ghosh MK, Kumar L, Roy C (2015) Monitoring the coastline change of Hatiya Island in Bangladesh using remote sensing techniques. ISPRS J Photogramm Remote Sens 101:137–144. https://doi.org/10.1016/j.isprsjprs.2014.12.009
- [19] Goldstein CA, Berry RB, Kent DT, et al (2020) Artificial intelligence in sleep medicine: Background and implications for clinicians. J Clin Sleep Med 16:609–618. https://doi.org/10.5664/jcsm.8388
- [20] Hagenaars G, de Vries S, Luijendijk AP, et al (2018) On the accuracy of automated shoreline detection derived from satellite imagery: A case study of the sand motor mega-scale nourishment. Coast Eng 133:113–125. https://doi.org/10.1016/j.coastaleng.2017.12.011
- [21] Hashemi S, Kiani S, Noroozi N, Moghaddam ME (2010) An image contrast enhancement method based on genetic algorithm. Pattern Recognit Lett 31:1816–1824. https://doi.org/10.1016/j.patrec.2009.12.006
- [22] Hewamalage H, Bergmeir C, Bandara K (2021) Recurrent Neural Networks for Time Series Forecasting: Current status and future directions. Int J Forecast 37:388–427. https://doi.org/10.1016/j.ijforecast.2020.06.008
- [23] Huang X, Li Y, Wang X (2024a) Science of the Total Environment Integrating a multi-variable scenario with Attention-LSTM model to forecast long-term coastal beach erosion. Sci Total Environ 954:176257. https://doi.org/10.1016/j.scitotenv.2024.176257
- [24] Huang X, Li Y, Wang X (2024b) Science of the Total Environment Integrating a multi-variable scenario with Attention-LSTM model to forecast long-term coastal beach erosion. Sci Total Environ 954:176257. https://doi.org/10.1016/j.scitotenv.2024.176257
- [25] Hyndman RJ, Koehler AB (2006) Another look at measures of forecast accuracy. Int J Forecast 22:679–688. https://doi.org/10.1016/j.ijforecast.2006.03.001
- [26] Ibrahim ASA, El Molla AM, Ahmed HGI (2024) Modeling Longshore Sediment Transport for Sustainable Coastal Management in the Damietta Port Area. J Eta Marit Sci 12:116–127. https://doi.org/10.4274/jems.2024.35119
- [27] Kamphuis JW (2010) Introduction to Coastal Engineering and Management, 2nd Edition. World Scientific
- [28] Karunarathna H, Horrillo-Caraballo J, Kuriyama Y, et al (2016) Linkages between sediment composition, wave climate and beach profile variability at multiple timescales. Mar Geol 381:194–208. https://doi.org/10.1016/j.margeo.2016.09.012
- [29] Kayri M (2016) Predictive abilities of Bayesian regularization and levenberg-marquardt algorithms in artificial neural networks: A comparative empirical

- study on social data. Math Comput Appl 21:20. https://doi.org/10.3390/mca21020020
- [30] Khalifa SAM, Elias N, Farag MA, et al (2019) Marine natural products: A source of novel anticancer drugs. Mar Drugs 17:491. https://doi.org/10.3390/md17090491
- [31] Krause P, Boyle DP, Bäse F (2005) Comparison of different efficiency criteria for hydrological model assessment. Adv Geosci 5:89–97. https://doi.org/10.5194/adgeo-5-89-2005
- [32] Legates DR, McCabe GJ (1999) Evaluating the use of "goodness-of-fit" measures in hydrologic and hydroclimatic model validation. Water Resour Res 35:233–241. https://doi.org/10.1029/1998WR900018
- [33] Luijendijk A, Hagenaars G, Ranasinghe R, et al (2018) The state of the world's beaches. Sci Rep 8:1–11
- [34] Mansour N, Sarhan T, El-Gamal M, Nassar K (2024) Assessing the compatibility of EPR rates with one-dimensional numerical modelling in monitoring shoreline kinematics along with supplying near/long-term forecasts. Reg Stud Mar Sci 71:103391. https://doi.org/10.1016/j.rsma.2024.103391
- [35] Masria A, Alshammari TO, Ghareeb M, et al (2024) 2D and 3D Modeling of Resistivity and Chargeability to Identify the Type of Saturated Groundwater for Complex Sedimentary Facies. Hydrology 11
- [36] Masria A, Esmail M, Tharwat Sarhan A, et al (2022) Management strategies for complex sedimentation process: a case study using remote sensing and morphodynamics simulation at Damietta Harbour, Nile Delta. Int J River Basin Manag 22:45–55. https://doi.org/10.1080/15715124.2022.2101463
- [37] Montaño J, Coco G, Antolínez JAA, et al (2020) Blind testing of shoreline evolution models. Sci Rep 10:1–10. https://doi.org/10.1038/s41598-020-59018-v
- [38] Moriasi DN, Arnold JG, Van Liew MW, et al (2007) Model evaluation guidelines for systematic quantification of accuracy in watershed simulations. Trans ASABE 50:885–900
- [39] Nandi S, Ghosh M, Kundu A, et al (2016) Shoreline shifting and its prediction using remote sensing and GIS techniques: a case study of Sagar Island, West Bengal (India). J Coast Conserv 20:61–80. https://doi.org/10.1007/s11852-015-0418-4
- [40] Nassar K, Fath H, Mahmod WE, et al (2018) Automatic detection of shoreline change: case of North Sinai coast, Egypt. J Coast Conserv 22:1057–1083. https://doi.org/10.1007/s11852-018-0613-1
- [41] Nielsen P, Callaghan DP (2003) Shear stress and sediment transport calculations for sheet flow under waves. Coast Eng 47:347–354. https://doi.org/10.1016/S0378-3839(02)00141-2
- [42] Oborie E, Francis O, Eteh D (2024) Amplitude Variation with Offset (AVO) Inversion for Reservoir Visualization: A Case Study of Taje Field, Niger Delta,

- Nigeria. Adv Geol Geotech Eng Res 6:21–32. https://doi.org/10.30564/agger.v6i1.6158
- [43] Pardo-Igúzquiza E, Dowd PA, Durán JJ, Robledo-Ardila P (2019) A review of fractals in karst. Int J Speleol 48:11–20. https://doi.org/10.5038/1827-806X.48.1.2218
- [44] Pawlowicz R, Beardsley B, Lentz S (2002) Classical tidal harmonic analysis including error estimates in MATLAB using TDE. Comput Geosci 28:929–937. https://doi.org/10.1016/S0098-3004(02)00013-4
- [45] Raja H, Omar W, Mounsif I, Duc M (2023) Coastal cliff failures hazard along the Safi coastline (Morocco): a methodology for shoreline change assessment and its forecast along with examination of the causes. Environ Earth Sci 82:255. https://doi.org/10.1007/s12665-023-10925-z
- [46] Revanesh M, Gundal SS, Arunkumar JR, et al (2024) Artificial neural networks-based improved Levenberg–Marquardt neural network for energy efficiency and anomaly detection in WSN. Wirel Networks 30:5613–5628. https://doi.org/10.1007/s11276-023-03297-6
- [47] Sahoo B, Bhaskaran PK (2019) Prediction of storm surge and coastal inundation using Artificial Neural Network A case study for 1999 Odisha Super Cyclone. Weather Clim Extrem 23:100196. https://doi.org/10.1016/j.wace.2019.100196
- [48] Shang D, Yan Z, Zhang L, Cui Z (2023) Digital financial asset price fluctuation forecasting in digital economy era using blockchain information: A reconstructed dynamic-bound Levenberg–Marquardt neural-network approach. Expert Syst Appl 228:120329. https://doi.org/10.1016/j.eswa.2023.120329
- [49] Simmons JA, Harley MD, Marshall LA, et al (2017) Calibrating and assessing uncertainty in coastal numerical models. Coast Eng 125:28–41. https://doi.org/10.1016/j.coastaleng.2017.04.005
- [50] Splinter KD, Coco G (2021) Challenges and Opportunities in Coastal Shoreline Prediction. Front Mar Sci 8:788657. https://doi.org/10.3389/fmars.2021.788657
- [51] Stanley DJ, Warne AG (1998) Nile delta in its destruction phase. J Coast Res 14:794–825
- [52] Tang L (2020) Application of Nonlinear Autoregressive with Exogenous Input (Narx) Neural Network in Macroeconomic Forecasting, National Goal Setting and Global Competitiveness Assessment. SSRN Electron J. https://doi.org/10.2139/ssrn.3601778
- [53] Taylor KE (2001) Summarizing multiple aspects of model performance in a single diagram. J Geophys Res Atmos 106:7183–7192. https://doi.org/10.1029/2000JD900719
- [54] Tharwat Sarhan A, Mina Iskander M, Nassar K, El-Gamal M (2022) Shoreline Changes Detection Using Digital Shoreline Analysis System: Case Study Damietta Port Said Coastal Area, Egypt. MEJ Mansoura Eng J 47:35–48. https://doi.org/10.21608/bfemu.2022.236869

- [55] Torres-Freyermuth A, Puleo JA, DiCosmo N, et al (2017) Nearshore circulation on a sea breeze dominated beach during intense wind events. Cont Shelf Res 151:40–52. https://doi.org/10.1016/j.csr.2017.10.008
- [56] Trageser JH, Elwany H (1990) The S4DW--An integrated solution to directional wave measurements. In: Proceedings of the IEEE Fourth Working Conference on Current Measurement. pp 154–168
- [57] Vidyalashmi K, L MC, Nandana JS, et al (2024a) Analyzing the performance of the NARX model for forecasting the water level in the Chikugo River estuary, Japan. Environ Res 251:118531. https://doi.org/10.1016/j.envres.2024.118531
- [58] Vidyalashmi K, L MC, Nandana JS, et al (2024b) Analyzing the performance of the NARX model for forecasting the water level in the Chikugo River estuary, Japan. Environ Res 251:118531. https://doi.org/10.1016/j.envres.2024.118531
- [59] Vitousek S, Barnard PL, Fletcher CH, et al (2017) Doubling of coastal flooding frequency within decades due to sea-level rise. Sci Rep 7:1399. https://doi.org/10.1038/s41598-017-01362-7
- [60] Vitousek S, Vos K, Splinter KD, et al (2023) A Model Integrating Satellite-Derived Shoreline Observations for Predicting Fine-Scale Shoreline Response to Waves and Sea-Level Rise Across Large Coastal Regions. J Geophys Res Earth Surf 128:e2022JF006936. https://doi.org/10.1029/2022JF006936
- [61] Vos K, Harley MD, Splinter KD, et al (2019) Sub-annual to multi-decadal shoreline variability from publicly available satellite imagery. Coast Eng 150:160–174. https://doi.org/10.1016/j.coastaleng.2019.04.004
- [62] Vousdoukas MI, Ranasinghe R, Mentaschi L, et al (2020) Sandy coastlines under threat of erosion. Nat Clim Chang 10:260–263. https://doi.org/10.1038/s41558-020-0697-0
- [63] Wulder MA, Loveland TR, Roy DP, et al (2019) Current status of Landsat program, science, and applications. Remote Sens Environ 225:127–147. https://doi.org/10.1016/j.rse.2019.02.015
- [64] Youssef YM, Gemail KS, Atia HM, Mahdy M (2024) Insight into land cover dynamics and water challenges under anthropogenic and climatic changes in the eastern Nile Delta: Inference from remote sensing and GIS data. Sci Total Environ 913:169690. https://doi.org/10.1016/j.scitotenv.2023.169690
- [65] Zeinali S, Dehghani M, Talebbeydokhti N (2021) Artificial neural network for the prediction of shoreline changes in Narrabeen, Australia. Appl Ocean Res 107:102362. https://doi.org/10.1016/j.apor.2020.102362